Analysis of acidity production during enhanced reductive dechlorination using a simplified reactive transport model

A. Brovelli [a,1], D. A. Barry [a], C. Robinson [a,c], J. I. Gerhard [b,c]

[a] Laboratoire de technologie écologique, Institut d'ingénierie de l'environnement, Faculté de l'environnement naturel, architectural et construit (ENAC), Station 2, Ecole Polytechnique Fédérale de Lausanne (EPFL), 1015 Lausanne, Switzerland. Emails: alessandro.brovelli@epfl.ch, andrew.barry@epfl.ch

[b] Institute for Infrastructure and Environment, University of Edinburgh, Edinburgh EH9 3JL United Kingdom.

[c] Now at: Department of Civil and Environmental Engineering, University of Western Ontario, London N6A 5B9, Canada. Emails: crobinson@eng.uwo.ca, jgerhard@eng.uwo.ca

Accepted for Publication in *Advances in Water Resources*

7 April 2012

[1] Author to whom all correspondence should be addressed Ph. +41 (21) 693-5919, Fax. +41 (21) 693-8035

Abstract

Build-up of fermentation products and hydrochloric acid at a contaminated site undergoing enhanced reductive dechlorination can result in groundwater acidification. Sub-optimal pH conditions can inhibit microbial activity and lead to reduced dechlorination rates. The extent of acidification likely to occur is site-specific and depends primarily on the extent of fermentation and dechlorination, the geochemical composition of soil and groundwater, and the pH-sensitivity of the active microbial populations. Here, the key chemical and physical mechanisms that control the extent of groundwater acidification in a contaminated site were examined, and the extent to which the remediation efficiency was affected by variations in groundwater pH was evaluated using a simplified process-based reactive-transport model. This model was applied successfully to a well-documented field site and was then employed in a sensitivity analysis to identify the processes likely to significantly influence acidity production and subsequent microbial inhibition. The accumulation of organic acids produced from the fermentation of the injected substrate was the main cause of the pH change. The concentration of dissolved sulphates controlled substrate-utilization efficiency because sulphate-reducing biomass competed with halo-respiring biomass for the fermentation products. It was shown further that increased groundwater velocity increases dilution and reduces the accumulation of acidic products. As a consequence, the flow rate corresponding to the highest remediation efficiency depends on the fermentation and dechlorination rates. The model enables investigation and forecasting of the extent and areal distribution of pH change, providing a means to optimize the application of reductive dechlorination for site remediation.

Keywords: reductive dehalogenation, source zone treatment, pH change, alkalinity, chlorinated ethenes, bioremediation, TCE

1. Introduction

Soil and groundwater contamination resulting from chlorinated solvents is a widespread problem, and significant efforts have focused on identifying and developing innovative remediation schemes. Chlorinated solvents degrade slowly in natural conditions and pose serious risks for the human health and the environment. A promising technology to treat this class of contaminants is enhanced in situ reductive dechlorination. With this technique, the activity of microbial consortia able to degrade chlorinated ethenes is stimulated in the solvent plume or in the proximity of the non-aqueous phase liquid (NAPL) source zone resulting in dechlorination and, in the latter case, an enhanced rate of dissolution and faster clean-up [1, 2].

Complete degradation occurs in a step-wise process, with tetrachloroethene (PCE) converted to ethene through a sequence of reactions and intermediate daughter chlorinated ethenes, i.e., trichloroethene (TCE), dichloroethene (DCE) and vinyl chloride (VC). During each step of the reaction sequence, one chlorine atom is removed. This in turn leads to a net production of hydrochloric acid (HCl), driving a decrease in the groundwater pH. The concurrent production of organic acids during fermentation of injected organic substrate further contributes to pH decline [3-5]. Soil minerals and the natural alkalinity of groundwater can – at least partially – counterbalance the progressive acidification [6, 7], as can mixing and dilution within the aquifer. Laboratory studies and field experiments have shown that enhanced dechlorination seldom completes with the lesser chlorinated solvents (DCE and VC) remaining in the soil and groundwater [5, 8-10]. The reasons for the inhibition have been widely investigated, with pH reduction implicated as a factor [1, 3-6].

The extent of soil and groundwater pH change can be significant and depends on the amount of dechlorination, site geochemistry and available microbial consortia. For example,

Sleep et al. [10], in a set of laboratory dechlorination experiments, observed a pH as low as 4.9, while Cirpka et al. [11], in a 2D tank experiment, measured a pH lower than 5.4. Leeson et al. [3, Appendix E.11] summarized measurements of groundwater pH for 50 chlorinated ethene-contaminated sites before and after clean-up. They reported a drop in pH in nearly all of the sites, with most of the values ranging from 5.5 to 7. In about 10 sites, the groundwater pH at one or more sampling locations was lower than 5, and in one case a pH of 3 was observed. The variability observed can be partially attributed to the specific geochemical conditions of different sites. For example, Lacroix et al. [12], evaluated the ability of silicates – which can be either naturally present in the soil or added during the treatment – to buffer groundwater pH. It was found that some minerals (such as nepheline, fayalite and glaucophane) can provide sufficient buffering capacity to counterbalance the acidity produced during dechlorination if they have a sufficient exposed reactive surface area.

Low pH conditions are not optimal for microbial activity, and the highest microbial dechlorination rate is normally observed in the near-neutral pH range of 6.5-7.5 [6, 12-15]. Based on these and similar laboratory experiments and several field studies, Leeson et al. [3] recommended maintaining pH in the near-neutral range, i.e., 6-8. In the same report, it was further stated that, depending on the geochemistry of the site and on the composition of the microbial consortia, a pH between 5 and 6 could still be acceptable. However, if the pH is lower than 5, pH adjustment is needed to maintain dechlorination. A low pH occurs when the acidity produced by the biological processes exceeds the soil and groundwater's buffering capacity. For continuing remediation, this buffering must be provided externally (e.g., [7, 12]).

Few detailed studies have been conducted to investigate acidity production and its effects on the degradation of chlorinated solvents. McCarty et al. [6] evaluated theoretically the amount of dechlorination expected before pH inhibition, considering numerous electron donors and initial groundwater alkalinities. Robinson et al. [7] and Robinson and Barry [16]

developed a more comprehensive geochemical model, including the effects of groundwater composition, competing terminal electron-accepting processes (TEAPs) and gas release, to calculate the expected acidification and the corresponding amount of buffer required. These models are based on a mass-balance approach that accounts for the main sources of acidity and of alkalinity, and provide – for batch systems – estimates of the amount of buffer required per unit concentration of chlorinated ethenes removed. However, these studies neglected water flow and mixing in the subsurface (i.e., they assume that the groundwater residence time is greater than the characteristic reaction time). This limits their applicability as design tools in practical situations, as they are unable to predict the areal distribution of the pH changes. On the other hand, more complex and comprehensive reactive transport models can be used. While able to predict in detail the areal distribution of all the chemical components – including pH – they have many unknown model parameters that are difficult to estimate or measure [17]. In addition, they are demanding computationally. For these reasons, they are best considered as research tools that are unsuitable for real field-scale applications. Instead, contaminated-site remediation design is often based on rules-of-thumb or simplified mass-balance calculations that potentially introduce significant errors.

The goal of this work was to develop a simplified mechanistic model to predict groundwater acidity build-up during enhanced reductive dechlorination that can be used as a tool to evaluate the expected changes in pH at chlorinated solvent-contaminated sites undergoing biological treatment. Included in the model were the processes that control (i) the amount of acidity produced, (ii) the natural buffering capacity of the soil and groundwater, and (iii) the time scales associated with these processes (§2). Several assumptions were introduced (§2) to limit the number of model parameters and the computational demand. These simplifications are evaluated and found to lead to conservative predictions; that is, it is expected that the modelled pH changes slightly overestimate the field

observations. To test its abilities and to show its practical application, the model was applied to a real contaminated site remediation scenario (§3) for which measurements of the main biogeochemical and hydraulic properties were available. A sensitivity analysis was conducted to elucidate the impact of different physical, biological and geochemical processes – and of the associated uncertainties – on the pH inhibition and remediation efficiency (§4).

2. Modelling approach

2.1. Fermentation and dechlorination

In enhanced in situ bioremediation schemes, a fermentable organic substrate is injected upstream of the site undergoing clean-up. Final fermentation products are hydrogen (H_2) and acetic acid. The model is a development of the geochemical reaction network presented by Robinson et al. [7]. Here we summarize the main equations and assumptions, as well as the modifications that were introduced. Considering linoleic acid (a commonly used substrate in field-scale applications), for example, the overall fermentation reaction stoichiometry is:

$$C_{18}H_{32}O_2 + 16H_2O = 9CH_3COOH + 14H_2 . \quad (1)$$

The weak organic acid, acetic acid, that is produced can accumulate and contribute to the acidification of the soil and groundwater. For this reason, the amount of acidity generated depends, among other things, on the specific fermentable substrate used [6]. Reaction stoichiometries for other commonly used substrates can be found in the literature [6, 7, 17].

H_2 is the primary electron donor for dechlorination. Following Robinson et al. [7], the model assumes a generic reaction between chlorinated organic ethenes (R-Cl) and H_2:

$$R\text{-}Cl + H_2 = R\text{-}H + HCl . \quad (2)$$

The HCl produced from this reaction is the other main source of acidity in groundwater undergoing dechlorination. Using the notation R-Cl, the same conceptual modelling framework can be applied regardless of the chlorinated ethene considered. For example, PCE, which contains 4 Cl atoms per molecule, is represented as 4R-Cl. The 4 refers to Cl, and R is simply to indicate that the Cl is part of a chlorinated compound. Observe that *n* moles of R-Cl degrade to *n* moles of R-H according to the dechlorination rate. Using a single generic reaction for all chlorinated ethenes means that compound-specific modelling of dissolution, sorption, and dechlorination rates is not possible. This approach, on the other hand, significantly reduces the computation burden and the number of model parameters required; two aspects that limit the application of detailed mechanistic models at the field scale [17, 18]. As will be shown in the results section (§3.4), the simplified model was able to reproduce correctly the pH changes observed in the field. When the model is applied as a design tool, the exact model formulation (i.e., the geochemical processes considered) and parameters must be chosen to guarantee that the rate of acidity production is never underestimated, that is, the fastest dechlorination rate (among those of PCE, TCE, DCE and VC) must be used. This way, the model produces a conservative estimate of the change in groundwater pH.

The acetic acid produced from electron donor fermentation can also be an electron donor for the reductive dechlorination of PCE to TCE and TCE to DCE [19-22], with a net production of CO_2 and HCl [7]:

$$4\text{R-Cl} + CH_3COOH = 4\text{R-H} + 4\text{HCl} + CO_2 . \quad (3)$$

The model described in this work considers only microbial degradation of chlorinated ethenes. In the presence of FeS, abiotic degradation can occur also [23-25]. Since this process generates acidity (hydrochloric and sulphuric acids are the reaction products, e.g., [23]), if

geochemical conditions are favourable or available experimental evidence shows its occurrence, the model should be extended to incorporate this degradation pathway.

The rates of fermentation and dechlorination were modelled using a simplified Monod equation, modified to account for pH inhibition [21], the only inhibition mechanism considered. This approach assumes that other processes causing inhibition (e.g., toxic concentration of chlorinated ethenes, lack of nutrients, etc.) remain constant during the simulated period and therefore do not affect the maximum reaction rate. This simplification neglects complex feedbacks that occur as dechlorination progresses. Nonetheless, a similar conceptualization of the dechlorination process as lumped first-order and simplified Monod kinetic reactions has been employed successfully in simulating numerous practical field-scale applications [18, 26, 27]. Reductive dechlorination is complex: Refined, process-based modelling requires detailed knowledge and understanding of the numerous reaction steps and kinetic parameters and is computationally demanding [17]. While such complex modelling would be useful to optimize site remediation or to understand the rate-limiting processes and enhance dechlorination, this work focuses on acidity production and natural buffering capacity, and a simplified approach is suitable. More importantly, as evident in the following sections, the kinetic parameters adopted provide valuable insight for identifying sites that are potentially more sensitive to acidity production. Since fermentation, dechlorination and acid production are closely linked, the rate parameters also indicate the time scale for acidity build-up.

In parallel to dechlorination, inorganic TEAs can consume part of the H_2 and acetic acid produced during fermentation. These processes influence groundwater pH as they remove acetic acid and produce alkalinity [6, 7]. For thermodynamic reasons, the primary competing terminal electron acceptors (TEAs) are sulphate and iron(III). Acetic acid oxidation via TEAPs was included as a rate-controlled process, while for H_2 consumption a two-step partial

equilibrium approach [19, 28, 29] was used. For this latter process, it was assumed that dechlorination is the rate-limiting step, while the reduction of competing TEAs can be approximated with equilibrium reactions [28, 29]. In practice, a parameter, $r_{D,min}$ $\left(0 \le r_{D,min} \le 1\right)$, was defined, which quantifies the dechlorination rate decrease if sulphate and iron(III) are present. Reduction of competing TEAs, considered to be equilibrium reactions, was simulated using the default thermodynamic values of the PHREEQC database [30]. This approach assumes that the concentrations of sulphate- and iron(III)-reducers in the aquifer remain constant.

The transformation rates for organic substrate fermentation (subscript *F*) and reductive dechlorination (subscript *D*) were computed as:

$$r_F = \mu_{max,F} \left(\frac{C_{aq,F}}{K_{h,F} + C_{aq,F}} \right) I_{\mathrm{pH}} B_F, \tag{4}$$

$$r_D = \mu_{max,D} \left(\frac{C_{aq,\mathrm{RCl}}}{K_{h,\mathrm{RCl}} + C_{aq,\mathrm{RCl}}} \right) \left(\frac{C_S}{K_S + C_S} \right) I_{\mathrm{pH}} B_D, \tag{5}$$

where μ_{max} [$M^{-1}\ T^{-1}$] is the maximum rate per unit biomass, K_h [$M\ L^{-3}$] the Monod half-saturation constant, I_{pH} is the pH inhibition factor, C_{aq} [$M\ L^{-3}$] the aqueous phase concentration (of the fermentable substrate, *F*, and chlorinated compound, RCl, respectively), C_S [$M\ L^{-3}$] the electron donor concentration (H_2 or acetic acid) and B [$M_b\ L^{-3}$] the biomass concentration (the subscript b denotes biomass). When competing TEAs are present, the dechlorination rate is reduced and becomes $r_D \times r_{D,min}$. Acetic acid tends to accumulate in the groundwater. The oxidation of acetic acid by competing TEAs [31] was also included as a kinetic process, modelled with a first-order reaction rate.

Following Ratkowsky and Ross [32], the pH inhibition relationship I_{pH} ($0 \le I_{pH} \le 1$) was modelled using a logistic function:

$$I_{\mathrm{pH}} = \left\{1 + \exp\left[M\left(\mathrm{pH} - D\right)\right]\right\}^{-v}, \tag{6}$$

where D, M and v are empirical parameters. Equation (6) was fitted to two groups of experimental data using least-squares minimisation (Fig. 1). The first dataset combines the observations reported by Holliger et al. [14] and Neumann et al. [15], while the second includes results from Zhuang and Pavlostathis [22]. The two resulting logistic pH inhibition functions were named I_{pH}^{HN} and I_{pH}^{Z}, respectively. The parameter values obtained from fitting Eq. (6) are reported in Table 1 along with correlation coefficients, while the datasets and the corresponding functions are shown in Fig. 1. At pH values greater than 6.7, the two functions are nearly identical. As the pH decreases, it can be seen that I_{pH}^{HN} decreases rapidly, approaching 0 (i.e., no microbial activity) when the pH is 6. In contrast, I_{pH}^{Z} decreases more slowly, with significant microbial activity ($I_{\mathrm{pH}} > 0.5$) at pH = 6, and a small amount of residual activity remains at pH = 4. However, Zhuang and Pavlostathis [22] further observed that, for pH < 6, DCE and VC accumulated in the column, thus suggesting a larger pH sensitivity for the final steps of the dechlorination reaction series. A review of the optimal pH ranges for dechlorinating microbial consortia is reported in [13], where it is shown that the range of pH where optimal conditions exist is relatively large, with some consortia maintaining high dechlorination efficiency when the pH is as low as 5.3. However, a pH above 6 is likely necessary to achieve complete degradation of TCE/PCE to ethene.

Two microbial consortia were considered, fermenters (B_F) and halo-respirers (B_D). The dehalogenating consortium (B_D) was assumed to be able to utilize both electron donors

(H_2 and acetic acid). The same pH inhibition function, Eq. (6), was assumed to hold for both consortia. This is a simplification since fermentation in soil is performed by several microorganism populations (including yeasts and fungi) that are active in a larger pH range than halo-respirers [33]. Numerical experiments (not reported) conducted using different inhibition functions suggested that the impact of this assumption is limited because the accumulation of organic acids is controlled mostly by other mechanisms. The rate of change in the biomass population, r_{B_i}, is a function of the degradation rate r_i, the yield factor, Y_i, and the first-order decay rate, k_d:

$$r_{B_i} = Y_i r_i - k_d B_i. \tag{7}$$

The fermentable organic substrate (e.g., soybean oil) is typically injected as an emulsion, but relatively quickly the oil becomes trapped as a separate phase around the injection well; oil dissolution provides on-going dissolved organics (e.g., linoleic acid) for fermentation. In addition, it is common for the chlorinated compounds to result from dissolution of NAPL pools and residual in the contaminant source zone. NAPL dissolution (injected oil and contaminant, i.e., TCE NAPL) was included as rate-limited interphase mass transfer using a unidirectional linear driving force approximation [31, 32]:

$$r_{diss} = -\mathrm{H}\left(\theta^0_{\mathrm{NAPL}}\right) k_{diss} \left(C^{eq}_{aq} - C_{aq}\right), \tag{8}$$

where θ^0_{NAPL} is the initial mass fraction of immobile NAPL (oil from injected emulsion or TCE), r_{diss} is the dissolution rate of the non-aqueous immobile phase, C^{eq}_{aq} is the solubility limit, C_{aq} is the concentration in the aqueous phase and k_{diss} is the dissolution rate parameter. The Heaviside function, $\mathrm{H}(\theta^0_{\mathrm{NAPL}})$, indicates that dissolution can occur only at locations where NAPL was present initially (superscript 0). Dissolution reduces the saturation of NAPL and

increases the aqueous phase concentration. Enhanced dissolution is reproduced correctly by this approach because aqueous concentrations of chlorinated ethenes (C_{aq}) will be decreased as R-Cl is biodegraded. This increases the driving force for dissolution. The dissolution parameter is a function of the mass-transfer coefficient, κ, and the specific interfacial area of the immobile phase, a. A modified version of the Powers model, which shows reasonable agreement with PCE dissolution data in soil columns and in the field [26, 34-36], was implemented. The dissolution rate was computed as:

$$k_{diss} = \kappa a_0 \left(\frac{\theta_{\mathrm{NAPL}}}{\theta^0_{\mathrm{NAPL}}} \right)^{\beta}, \tag{9}$$

where θ_{NAPL} is the current mass fraction of NAPL, β is an empirical exponent dependent on the properties of the porous medium, and a_0 is the initial interfacial area. This latter value can be estimated based on geometrical considerations [35, 37, 38] and the average grain size of the porous medium. The mass-transfer coefficient was assumed constant in all the simulations, thus neglecting the possible production of bio-surfactants.

2.2. Gas phases

Fermentation results in net production of dissolved CO_2, as shown by Eq. (3). Dissolved CO_2 can potentially be released as a gas, depending on the water composition and groundwater depth. Since dissolved CO_2 alters the carbonate equilibria, it also affects the pH and buffering capacity of soil and groundwater. In the model, a gas phase was allowed to form when the sum of partial pressures of all the gases (N_2, O_2, CO_2, H_2, H_2S, CH_4, H_2O) exceeded the hydrostatic pressure.

Methanogenesis was also considered in the model. Methane production can occur via cleavage of acetic acid or direct use of H_2 (e.g., [31, 39]):

$$CH_3COOH = CH_4 + CO_2, \quad (10)$$

$$2H_2 + CO_2 = CH_4 + 2H_2O. \quad (11)$$

The effect of methanogenesis on pH, while non-trivial, is relatively weak overall. Acetate cleavage removes acidity from the solution but adds CO_2, thus shifting the carbonate equilibria (or producing gaseous CO_2), while the use of H_2 removes CO_2 from the groundwater and shifts the carbonate equilibria in the opposite direction. Both reactions were modelled as kinetic processes, with a first-order reaction rate (Eq. 12). The effect of pH on the rate of methanogenesis was neglected. While some researchers have observed complete inhibition of methanogenic Archea at low pH (< 5.5) in peat [40] and rumen [41, 42], methane efflux is often measured in situations with high organic acid concentrations and low pH [43]. The occurrence of methanogenesis even in acidic groundwater was attributed to the presence [44] of low pH-tolerant methanogenic strains in the soil [43]. This was further confirmed by the lack of correlation between groundwater pH and methane production in the experimental data used in this work. Several investigators have found that methane production is inhibited in the presence of high PCE/TCE aqueous concentrations or NAPL [e.g. 2, 44]. For this reason, a switch function was introduced in the rate equation to halt methanogenesis when the aqueous concentrations of the chlorinated compounds exceed a threshold value ($C_{\mathrm{RCl}}^{switch}$) (e.g., 0.5 mM [2]), so that the final rate is given by:

$$r_{\mathrm{CH_4}} = \left[1 - \mathrm{H}\left(C_{\mathrm{RCl}} - C_{\mathrm{RCl}}^{switch}\right)\right] k_{\mathrm{CH_4},S} C_S, \quad (12)$$

where C_S is the concentration of electron donor (methane or acetic acid).

2.3 Mineral phases

Changes in the pH and the solution composition can result in precipitation and dissolution of soil minerals, which can subsequently alter the groundwater alkalinity. The model includes dissolution and precipitation of calcite, an important buffering mineral, due to its influence on carbonate equilibria. The following rate expression was used [39, 45]:

$$r_{\mathrm{CaCO_3}} = k_1\left[\mathrm{H^+}\right] + k_2\left[\mathrm{H_2CO_3}\right] + k_3\left[\mathrm{H_2O}\right] - k_4\left[\mathrm{Ca^{2+}}\right]\left[\mathrm{HCO_3^-}\right], \quad (13)$$

where the parameters k_1, k_2, k_3 and k_4 are temperature-dependent reaction rates, the values of which are taken from [39].

Also accounted for in the model are dissolution and reduction of iron oxides (goethite and ferrihydrite), and precipitation of iron sulphide resulting from sulphate and iron(III) reduction. These processes add alkalinity to the solution while consuming H_2 [7]. Iron sulphide is assumed to be in equilibrium with the solution [7, 39], while iron oxide reductive dissolution – due to its slow kinetics – is modelled as a rate-limited reaction [39]:

$$R_{\mathrm{Fe}} = k\frac{A_0}{V}\frac{m}{m_0}10^{-0.45\mathrm{pH}}, \quad (14)$$

where k is the rate constant, A_0 is the initial surface area of iron oxides, V is the solution volume, and m_0 and m are the initial and current undissolved amounts of iron oxides, respectively. The model does not account for the effect of iron(III) reducers on the precipitation/dissolution of Fe(III), as observed by [46, 47].

Experiments and numerical modelling in clayey formations [48] have shown that clay minerals have the ability to buffer the pore water pH, mainly via cation exchange (proton adsorption and release of alkali ions) [49]. Numerical experiments conducted in this work

(results not shown) suggested that the buffering capacity of clays becomes important when $pH < 5$. Given the uncertainties associated with this mechanism (lack of knowledge of the characteristics and sorption capacity of the clay), and the relatively limited importance in the pH range of interest for biological transformations (i.e., $5.5 \leq pH \leq 7.5$), its influence was neglected in the modelling presented below. In terms of treatment scheme design for contaminated sites, this assumption is conservative as it would result in a slight over-estimation of the pH decrease. Adsorption on hydrous ferric oxide (goethite and ferrihydrite, Hfo) can instead provide some buffering even in mildly acidic conditions ($pH < 6.5$) through proton complexation and exchange [39, 49]. The amount of buffering capacity depends upon the pore water composition and mass of Hfo in the soil. In this work, the Dzombak and Morel [50] model and database were used to simulate complexation on Hfo.

3. Model application

3.1. Site description

The model was applied to data from a pilot test conducted at the Altus Air Force Base (AAFB), Altus, Oklahoma, USA. Investigations in the early 1990s found different spots with high concentrations of chlorinated solvents within the AAFB. Details of the fieldworks and reports of the geological and geochemical characterizations pertaining to this site are available, as well as the results of the after-treatment monitoring ([51-53] and references therein). In this work, we focused on one contaminated location where a remediation scheme – named Pilot Plant #1, area SS-17 – was implemented and monitored [51]. The model was not applied with the intention to reproduce in detail all the available data. Rather, this site was used as an example of a realistic site with complex geology. The model was applied to investigate whether the model predictions were consistent with the field data (i.e., if the

predicted pH change was compatible with field observations) and to identify the parameters and processes that influence strongly the groundwater pH predictions.

The contamination source was a building adjacent to the pilot plant location where maintenance facilities were located. Monitoring activities revealed that contamination existed within the saturated zone, and extended to low permeability bedrock. The average hydraulic conductivity was approximately 0.1 m d^{-1} with a large variability (about two orders of magnitude in a small area of 10 m × 35 m). Porosity was varied in the range 0.31-0.38. In most of the area, measured organic carbon concentrations were low, while sulphate concentrations were significant and showed a high degree of spatial variability. This was related to the presence of a nearby layer of nearly pure gypsum, which is important because high sulphate concentrations lead to unfavourable conditions for reductive dechlorination: Halo-respirers are out-competed by sulphate-reducers for the fermentation products. The geochemical characterization, however, showed that natural microbial oxidation of BTEX from an adjoining fuel spill removed dissolved oxygen, nitrates and a fraction of the sulphates from the groundwater, therefore contributing to improved conditions for reductive dechlorination. Furthermore, data indicated that TCE degradation was already occurring prior the commencement of the remediation activities; this suggests (i) favourable geochemical conditions and (ii) the presence of a microbial consortium adapted to anaerobic respiration of chlorinated ethenes.

The treatment scheme consisted of fermentable substrate injection (emulsified soybean oil) to create a permeable reactive barrier and to stimulate the activity of halo-respiring biomass. Fig. 2 shows a schematic outline of the site (plan view). In total, 17 wells were placed in the area but, for clarity, only seven are shown in Fig. 2: The five injection boreholes and the monitoring well that were used to compare with model output. The monitoring location considered was the only place outside the injection barrier where a pH change (although very

small, about 0.3 pH units) was detected. The pH changed here because fermentation products reached the well. This could indicate that this was the only monitoring well directly connected hydraulically to the injection barrier. About a third of the ground surface was paved, thus preventing the vertical infiltration of water. The fermentable substrate was injected through the boreholes shown in Fig. 2 (closed circles, TS-IW-1 to TS-IW-5), aligned perpendicular to the groundwater flow direction. Downgradient, where the largest concentrations of dissolved TCE were measured, monitoring wells tracked the evolution of groundwater composition and gas production. The emulsion injection was divided into four batches, with each batch injected within a short period (about 8 to 12 h). The emulsion contained soybean oil as the organic substrate, an emulsifying agent, yeast extract as a nutrient amendment and sodium lactate as a subsidiary fermentable substrate. As the amount of sodium lactate injected in the aquifer was small compared with that of soybean oil, in the following it is assumed that biomass uses only the soybean oil. The volume of injected emulsion provided sufficient organic carbon and supported biodegradation/reduction of competing TEAs for a period of at least 3 y. Monitoring activities were conducted at six monitoring locations and five injection wells. Data from five downgradient monitoring wells, however, were not considered in the model application because either they showed negligible pH change or the pore water pH was not measured. At the locations where pH did not change in time, model predictions were consistent with experimental observations. The first monitoring event was conducted immediately before the injection to establish baseline conditions, the second shortly after the injection, and then four more were conducted in the following 2 y.

3.2. Model setup and initial conditions

As mentioned above, measured hydraulic properties at AAFB showed high spatial variability. This variability is likely to have a profound impact on both the time and spatial evolution of the reactive processes and, ultimately, on solute concentrations and remediation

efficiency. It follows that a detailed model comparison with a field data set is possible only if the heterogeneous distribution of the chemical and physical properties of the subsurface is characterized with sufficient resolution, and incorporated in the model. This is not the case in general because field measurements are sparse and resolution of the geochemical parameters in time is coarse. While the AAFB site is perhaps an extreme case, in all field situations there is a degree of heterogeneity that is impossible (or at least very difficult) to characterize. It is then useful to investigate whether a simplified 'physical' representation, wherein the effect of heterogeneity is neglected, can still provide realistic estimates of the pH change (as well as of the other geochemical processes). In other words, to determine whether spatially averaged rates (for flow and biogeochemical transformations) are able to give predictions compatible with the observations. In this respect, the highly heterogeneous AAFB case represents a challenging case study.

At a nearby site, Kennedy et al. [23] conducted investigations to quantify the extent of natural abiotic degradation of chlorinated solvents. They observed complete TCE removal, and they did not observe DCE and VC formation. This suggests that geochemical conditions at the AAFB site (presence of iron(III) and sulphates) are favourable for abiotic degradation. Oxygen levels were very low prior to the injection of fermentable organic matter [51], raising the possibility of abiotic degradation. However, the high TCE and low acetylene concentrations indicate that abiotic degradation was negligible before the treatment. After the injection and throughout the monitoring period, measured acetylene concentrations remained very low and did not show temporal variations [51], which further indicates that abiotic dechlorination did not occur 52]. In addition, previous studies indicate that abiotic degradation is pH-sensitive, with higher rates in the alkaline range [24, 25]. This suggests that, during the treatment, acidity generated by fermentation likely reduced further the contribution of abiotic degradation. For these reasons, abiotic degradation was neglected.

The domain modelled is a 15-m long 1D transect parallel to the flow direction that crosses the reactive permeable barrier near the central injection well, TS-IW-3. The location of the transect and its longitudinal extent are illustrated in Fig. 2 (dashed black line). Measurements show that most pH change occurs near the injection wells ([51], Table 4.10), probably due to the presence of the fermentable substrate. The model was tested using, in particular, the measurements at all injection wells for a 2-y period, specifically the concentrations of chlorinated ethenes, organic acids and TEAs dissolved in groundwater and methane produced. Moreover, one downstream monitoring well (TS-MW-5) was also considered outside the injection barrier, which is the area where most of the biogeochemical changes were expected. Fixed head boundary conditions were used at the inlet and outlet of the modelled domain, with head values computed from the average measured hydraulic gradient [51]. This is an approximation, but comparison with experimental data showed that this assumption is acceptable for simulating the long-term behaviour. Substrate injection was not simulated directly, but rather it was assumed that the emulsion reaches the aquifer instantaneously. This is reasonable because the length of the injection period (< 12 h) was short compared with the total simulation time (800 d), and consequently the disturbance induced on the flow field was insignificant. The emulsion in the aquifer behaved as a separate immobile phase that dissolved in the groundwater and moved downgradient accordingly. It is not clear from the data how far from the well the emulsion spread during the injection, and estimation was difficult due to the heterogeneous conditions of the aquifer [51]. Here it was assumed that the emulsion was present as an immobile phase within 3.5 m downgradient of the injection well, which was estimated on the basis of the amount of substrate injected (about 473 l).

Table 2 reports the main physical and geometrical properties of the transect. The hydraulic conductivity and porosity are average values [51]. The pressure in each cell was

calculated assuming hydrostatic conditions. This was required to compute the amount of gases that form as a separate phase when total of the dissolved phase gas partial pressures exceed the hydrostatic pressure. The longitudinal dispersivity for the site was unknown; to account for the rather large spatial variability of hydraulic conductivity, a value comparable to the grid spacing was assumed [39]. Table 3 lists the composition of the groundwater used to define both the initial condition and the background water at the transect inflow during the simulation. All the key values (sulphate, iron and alkalinity) were measured, and the concentrations used in the model were the average values of those observed in the field. Note, in particular, the very high concentration of sulphates and the negligible concentration of dissolved oxygen and nitrates, indicating that sulphate reduction was the dominant competing TEAP occurring at the site. Major cations were not measured in the groundwater and realistic amounts were added with the resulting solution equilibrated in the geochemical model PHREEQC [39].

Table 4 reports the initial amount of immobile components in the model. The pilot site was located about 80 m downgradient from the original spill site and it is probable that TCE was mainly present as dissolved phase in the groundwater. The initial amount of calcite was not measured. Since the available data indicated no (or limited) soil buffering capacity, the initial calcite concentration was set to a small value. This could mean, for example, that the formation was originally poor in carbonates and that the natural dechlorination had slowly consumed most of the system's natural buffering capacity, leading to a system sensitive to pH changes. On the other hand, the total amount of bio-available iron oxides was available from direct measurements, but with unknown composition (relative fractions of goethite and ferrihydrite). The composition of iron oxides was first modelled based on generic literature values [39], but with poor results. Consequently, this parameter was calibrated and a sensitivity analysis was performed to understand its effect on (i) the concentration of

dissolved iron and (ii) the groundwater pH. The parameters of the biogeochemical model including rates and inhibition factors are listed in Table 5.

The model was implemented using PHAST [54], a saturated flow and reactive transport computer code. PHAST couples HIST3D for groundwater flow and solute transport with the geochemical software package PHREEQC via a split-operator algorithm [21]. Numerical experiments were conducted to identify the optimal time step size and minimize the splitting error. For the setup used here, PHREEQC could have been employed directly. However, it was found that PHAST is computationally more efficient. Moreover, the same model will be applied to 2D and 3D scenarios in future studies and it was convenient to implement it directly within PHAST.

3.3. Model calibration

Field monitoring data were available for several components, but with a low sampling frequency. Trying to match all the measurements would likely result in an over-fitting of the model, given the large number of parameters that can be tuned compared with the number of experimental data. An approach was employed in which (i) most input parameters were derived from the site experimental data or studies showing comparable conditions, and (ii) calibration of the remaining parameters was constrained to stay within the ranges reported in the literature. An automated calibration using a Monte Carlo method was initially trialled, but this was found to be computationally expensive. This was due to (i) the number of parameters to be calibrated, (ii) the high correlation between some parameters, and (iii) the low sensitivity to some parameters, which results in a very large parameter space to be explored. More importantly, the results of the automatic calibration were found to be biased by a few measured values that the simulations were unable to reproduce. It is not possible to ascertain whether this was due simplifications in the model (e.g., the constant hydraulic gradient) or to

errors in the measurements. A manual trial-and-error approach was therefore used, keeping in mind the aim of reproducing the overall trends observed in the measurements. The manual approach was guided by the results of the automated calibration in that the more sensitive parameters were adjusted first.

The rate parameters controlling the availability of organic fatty acids (acetic acid) in groundwater were the most influential, in particular the fermentation rate and the acetic acid consumption rates (both dechlorination and sulphate reduction). The model was less sensitive to the parameters that control the dechlorination rate using H_2 as the electron donor, but nonetheless these parameters needed to be adjusted carefully. Since fermentation and dechlorination rates are sensitive to pH changes, the maximum degradation rates ($\mu_{max,D}$ and $\mu_{max,F}$) were calibrated considering mainly the measurements conducted with pH in the nearly neutral range. By doing this, calibration of the degradation rates and of the pH inhibition function could be done sequentially. Estimated model parameters and corresponding literature ranges (when available) are reported in Table 5.

The model results were sensitive to the pH inhibition function. Poor calibration results suggested that neither inhibition function, I_{pH}^{Z} nor I_{pH}^{HN}, was suitable for the case considered. Instead, a new logistic function with an intermediate behaviour (dashed line in Fig. 1, I_{pH}^{AFB}) was defined, the parameters for which are listed in Table 1. The main features of the new function are that (i) it closely reproduces both datasets at pH $>$ 6.5, with very low inhibition, (ii) at a pH of 6 the inhibition factor is about 0.5, similar to the results of [22], and (iii) when the groundwater is more acidic (pH $\leq$ 5.5) biomass activity drops to 0. Several environmental factors are likely to influence the biomass sensitivity to pH; for example, the composition of the microbial consortium and other environmental variables (temperature, redox potential, availability of nutrients, etc.). It should also be noted that the three datasets, [14], [15] and

[22], used to define the inhibition function might not be representative because, first, they pertain to laboratory experiments rather than a field case and, second, only dechlorination was used to recover the activity rate. It is unknown whether the high pH sensitivity of DCE/VC and VC/ethene transformations observed in the laboratory experiments [22] also applies in the field. If so, the use of the function I_{pH}^{HN} could be more appropriate. The influence of the pH inhibition function used on the dechlorination extent is investigated in §4.

3.4. Comparison with experimental data

Simulation results are presented and compared to the experimental data in Figs. 3-6. Fig. 3 reports the evolution of water chemistry near the injection wells: dissolved chlorinated ethenes in the upper panel, pH in the middle plot and acetic acid concentrations in the bottom panel. The mean and standard deviation of the measurements at all injection wells were computed, and are reported in the figures. The fermentation products (organic acids) measured in groundwater were acetic (main component), propionic and butyric acids, whereas in the model only acetic acid was considered. To facilitate the comparison between modelled and measured concentrations, the measured organic acids were converted to the corresponding concentration of acetic acid, preserving the total concentration of carboxylic (-COOH) groups. This may introduce a small inaccuracy in the solution pH because the dissociation constants of the organic acids produced by fermentation are slightly different.

Fig. 3 illustrates that the model provided a reasonable prediction of gross chlorinated ethenes and organic acids concentrations along the transect, as well as the pH trend. The main discrepancy is related to the R-Cl concentrations up to about day 240 d following the injection of the organic fermentable substrate. The measurements indicate that the concentration of dissolved chlorinated ethenes dropped quickly to about 1 μM, while the model predicts negligible dechlorination. The good match observed for pH and organic acids suggest that the

change in pH was due to the accumulation of acetic acid. Borden et al. [51] and Lee et al. [52] attributed the sharp drop in the concentration of the dissolved chlorinated ethenes to their partitioning into the oil emulsion, a process that was not considered in the model. The model predicted that dechlorination was weak initially and accelerated only after about 270 d; such an acclimation period is typical for bioremediation studies (e.g., [2, 44]). Both hypotheses are consistent with the fact that dechlorination by-products (DCE, VC and ethene) were not observed near most injection wells in the first sampling period, about 30 days after the oil injection [51]. While there is a discrepancy in predictions of chlorinated ethenes, whether due to partitioning into oil and/or low initial biodegradation rates, the actual mechanism is of low importance as the net effect on pH is the same.

The simulated acetic acid concentration reached a maximum about 75 d after the injection, then remained almost constant until 175 d. According to the model, in this period the inhibition of the microbial activity was due to the development of acidic conditions. In the following period, the fermentable substrate (as a separate oil phase) was consumed entirely, fermentation halted and acetate-consuming processes (mainly sulphate reduction, dechlorination and acetate cleavage) slowly removed organic acids from the subsurface. The groundwater pH mimicked closely acetic acid dynamics, suggesting that organic acids were the most important sources of acidity at the AAFB site. In addition, this also indicates that the soil natural buffering capacity was depleted and that other buffering mechanisms – e.g., clay dissolution – were negligible.

The measured concentration of methane was also well reproduced in the simulations (Fig. 4, upper plot), indicating that the underlying first-order kinetic model was suitable to capture the increasing trend observed in the field. Moreover, the measured methane concentration does not correlate negatively with groundwater pH, as reported elsewhere [22, 43].

Fig. 5 reports the modelled and predicted dissolved sulphate. The comparison is not entirely satisfactory, although near the injection well (open triangles and dashed line) the order of magnitude of the concentration and the overall trend are reproduced correctly. The sulphate concentration is controlled by reduction processes, and perhaps by the dissolution of gypsum, which is abundant at the AAFB site [51]. Numerical experiments were conducted to ascertain the importance of this latter process. It was found that gypsum dissolution did not improve significantly the model predictions of the sulphate dynamics. This suggests that the discrepancies are due to the equilibrium approximation used to simulate sulphate reduction and to the heterogeneous distribution of sulphates in the system. The very large standard deviation of the measurements observed at the injection wells support this last hypothesis.

The comparison of simulations and field measurements at monitoring well TS-MW-5 is satisfactory also. Fig. 6 reports dissolved chlorinated ethenes, pH and organic acids, while Figs. 4 (bottom panel) and 5 show the concentrations of methane and dissolved sulphates. For all components, the trend observed in the field was reproduced by the model, albeit with some discrepancies for sulphates. The pH change at this sampling location was small, and has in practice no influence on the biological activity (the groundwater pH always remains in the optimal range, above 6.5). Acetic acid was, again, responsible for the small pH change measured, but its peak concentration was less than 10% of the concentration at the injection well. Dissolved sulphate showed an initial increase that the model was unable to explain. Gypsum dissolution was again excluded because, at least in the model, groundwater was already supersaturated (the initial saturation index was about 0.7). Afterwards ($t > 400$ d), sulphate concentrations decreased, and the model predictions were consistent with field observations. Heterogeneity in sulphate distribution is one source of uncertainty, but it is difficult to reach any conclusion about the processes that control sulphate dynamics.

4. Sensitivity analysis and evaluation of remediation efficiency

4.1. Metrics

A sensitivity analysis was performed to identify the processes that influence the build-up of acidity in the groundwater and consequently on the dechlorination efficiency. This analysis was conducted to predict more reliably the circumstances that might result in groundwater acidification for a contaminated site undergoing remediation via enhanced reductive dechlorination. A number of scenarios were compared with a base-case defined by the model calibrated to the AAFB field data. However, to explore the effect of dechlorination on pH and to simulate source-zone remediation (for which groundwater acidification is more likely [6]), a residual NAPL saturation of 1.5% was included. In contrast to the results presented above, both fermentation products and HCl accumulate in groundwater and affect the pH. The following metrics were used to compare the different scenarios:

1. Total dechlorination. To evaluate the overall efficiency of the treatment/remediation scheme, the total amount of R-Cl degraded during the simulation period over the modelled transect was computed:

$$D_{R-Cl} = \iint R_{R-Cl}(x,t)dxdt\,, \tag{15}$$

where $R_{\text{R-Cl}}(x,t) > 0$ is the spatially dependent degradation rate of the chlorinated compounds using both linoleic acid and acetic acid as substrates. Due to the equivalent stoichiometric factor, the dechlorination efficiency metric also indicates the total HCl produced, and is a useful indicator to assess the relative contribution of HCl to acidification compared to acetic acid.

2. Total pH change. The extent of acidification was measured as the total change in pH across the simulated domain, and computed as the difference between the (constant) pH of the inflowing groundwater (pH^0) and the local pH:

$$D_{\mathrm{pH}} = \int \mathrm{pH}^0 - \mathrm{pH}(x,t)dx\,. \tag{16}$$

This index provides a quantitative measure of the decrease in groundwater quality and deterioration of the environmental conditions for microbial activity.

3. Minimum pH. The above value gives an indication of the total amount of acidity produced. However, the variations in microbial activity depend on the local pH, and the evolution of the minimum pH was also monitored using:

$$\mathrm{pH}_{min} = \min_{0\le x\le d} \mathrm{pH}\left(x,t\right), \tag{17}$$

where d is the length of the model (15 m, Table 2).

4. Numerical experiments indicated that the groundwater flow rate can limit acidification from dechlorination, due to dilution of the fermentation and dechlorination products (i.e., acetic acid and HCl). To quantify the relative magnitude of the groundwater flow rate for each scenario the dimensionless (first) Damköhler number (*Da*) was used [17]:

$$Da = \frac{r_c}{\tau}\,, \tag{18}$$

which is the ratio between the characteristic reaction rate (r_C) and the advective mass transport rate (τ). In the following, this value is computed as the ratio between the maximum dechlorination rate possible given the initial concentration of biomass, B_D [M T^{-1}] and the mass flow:

$$Da = \frac{\mu_{max,D} B_{0,D}}{Q C_{\mathrm{R-Cl}}}, \tag{19}$$

where Q is the volumetric flow rate in the model [$L^3\,T^{-1}$] and $C_{\mathrm{R\text{-}Cl}}$ [$M\,L^{-3}$] is the (constant) dissolved concentration of chlorinated ethenes in the groundwater (initial and inflow). The two main acid-generating processes (fermentation and dechlorination) occur with different rates and with reaction parameters that change in both time and space. Here, these parameters are assumed constant, and so the resulting Damköhler number is an approximation.

4.2. Effect of flow rate

During dechlorination, changes in pH are due mainly to the accumulation of fermentation products and hydrochloric acid in the aquifer. It is, therefore, reasonable to expect that changes in the flow rate will influence the acidity build-up. This effect was analysed by progressively increasing the hydraulic conductivity in the AAFB model setup. In the base case the averaged measured hydraulic conductivity value was used (0.1 m d^{-1}, [51] and Table 1). This value results in a very high Damköhler number ($Da \approx 1200$), meaning that the reaction rate is much larger than the advection rate, and reaction products accumulate in the aquifer, as also observed in the AAFB site simulations. The hydraulic conductivity was progressively increased up to 100 m d^{-1}, so that Da decreased to about 1. While this value of hydraulic conductivity might not be realistic under natural conditions, an increase in the flow rate can be obtained by changing the hydraulic gradient (e.g., using a groundwater control system), and the resulting advection rate used to compute Da is realistic for some field-scale applications.

The results of this suite of numerical experiments are shown in Fig. 7. The values were normalized using the metrics at $Da = 1$. The left panel reports the total pH change at 180 d

computed using Eq. (16), while the right panel illustrates the corresponding extent of dechlorination (Eq. 15). The two metrics show a similar pattern. The total amount of chlorinated ethenes degraded and total pH were constant for high *Da* ($Da \gtrsim 100$), steadily decreased with decreasing Damköhler number (i.e., increased groundwater velocity) and again remained constant at low *Da* ($Da < 5$). Constant values for the two metrics occur when the R-Cl removal stalls. At high flow rates, the electron donor produced by fermentation is flushed rapidly away from the site and its limited availability hinders dechlorination. In contrast, at high *Da,* the electron donor remains available to dehalogenators, but acidic reaction products also accumulate and the reaction stops.

The effect of flow rate on groundwater pH is investigated further in Fig. 8, which shows the evolution of the lowest pH in the modelled transect. Within the time scale of the simulations, the minimum pH is sufficient for continuing dechlorination (pH > 5.5) for $Da < 10$. Around this *Da*, electron donors remain in the system long enough to permit dechlorination, but the flow rate is such that acids are flushed and the pH remains acceptable. For $Da > 10$, the increased availability of electron donor promotes dechlorination, with larger production of acids. At the same time, the total pH change increases (Fig. 7) and the minimum pH decreases. The consequence of this negative feedback is that the extent of dechlorination does not increase linearly with the flow rate.

Based on these observations it was concluded that the groundwater flow rate strongly controls both the remediation efficiency and the degree of acidification likely to occur at a site undergoing enhanced bioremediation. For $Da > 50$, the influence of flow rate is negligible and the extent of acidification depends primarily on the extent of dechlorination and soil buffering capacity. In contrast, for $Da < 5$ the electron donors are diluted and transported rapidly downstream of the treatment zone, and consequently dechlorination is ineffective. Optimal degradation will be achieved with *Da* in the intermediate range, because the flow rate will

provide enough electron donor while diluting the acids. For a heterogeneous site, flow rates and hence *Da* varies, in which case bioremediation efficiency would likely vary spatially also.

4.3. Sensitivity to pH inhibition

As noted above, that there have been several laboratory investigations on the effect of pH on dechlorination rate. From both these and field experience, for effective remediation it is often recommended to maintain pH $\geq$ 6.5 (e.g., [6, 7] and references therein). Here we examine the extent to which the pH inhibition of biomass activity influences the amount of dechlorination, as well as the level of uncertainty in the simulation results. To this end, four simulations were performed. The base case was again defined by the model calibrated on the AAFB site with 1.5% TCE NAPL saturation, using the inhibition factor I_{pH}^{AFB} (Table 1 and Fig. 1). A second simulation was run assuming that reductive dechlorination was not inhibited by acidic conditions. This scenario is not realistic but was conducted to identify the pH baseline, i.e., the potential for groundwater acidification without any natural soil buffering capacity and feedback of acidic conditions on microbial activity. A pH of 2.2 was reached in this simulation. Two other simulations were performed using the pH inhibition functions I_{pH}^{Z} and I_{pH}^{HN} (Table 1 and Fig. 1). As noted above, the function I_{pH}^{HN} may be applicable if additional field studies confirm that dechlorination of DCE and VC only occurs for pH $>$ 6 [22]. The results are compared in Figs. 9 and 10. Figure 9 shows the total pH change within the transect (upper panel) and the amount of transformed R-Cl. Results were normalized using the largest value to facilitate the comparison. Not surprisingly, there is a difference in terms of dechlorination among the three functions. This analysis indicates that the model results are sensitive to the chosen function because the amount of acidity produced is very high. The comparison with the function used for the AAFB case, I_{pH}^{AFB}, shows total dechlorination comparable with that obtained using the broader inhibition function, I_{pH}^{Z}. The reason is that pH remains mostly

above 5.5, where the two functions are similar. Results obtained using I_{pH}^{HN} indicate a lower total dechlorination and smaller pH change, which occurs because I_{pH}^{HN} is the most sensitive to pH changes (dechlorination stops at pH ≈ 6).

4.4. . Soil and groundwater composition

As summarized in the introduction, a number of geochemical processes might contribute to buffer the acidity produced. Carbonate minerals are often present in soils, and their buffering effect might be key for successful remediation [6, 7]. At the AAFB site, although the amount of calcite was not reported, the measurements showed fast pH variation, indicating limited availability of soluble carbonates. An additional simulation was conducted to evaluate to what extent increased calcite availability reduces the pH drop. The alternative scenario (named C_B) was similar to the base case (C_A), but with more calcite (initial $CaCO_3$ was, respectively, 10^{-3} and 5×10^{-1} mol (kg soil)$^{-1}$ for C_A and C_B) available in the aquifer. As expected when substantial calcite was present, the groundwater acidification was significantly smaller (Fig. 11, top panels). While in the base case the minimum pH was close to 5, calcite buffering in the alternative scenario resulted in groundwater that is only mildly acidic (pH ≈ 6.3). This difference in groundwater acidification influenced both fermentation and dechlorination reactions, and the time required to remediate the site.

The importance of sulphate concentrations was evaluated considering two groundwater compositions with the same alkalinity (6.8 meq l^{-1}) and major ions, although with different sulphate concentrations (6.25×10^{-2} mmol l^{-1} and 12.5 mmol l^{-1}, cases S_A and S_B, respectively). Since at the AAFB site the source of sulphates is gypsum ($CaSO_4 \cdot 2H_2O$) dissolution, the concentration of Ca^{2+} was equilibrated using PHREEQC to attain charge balance. The initial pH of the two solutions was slightly different (7.0 and 6.7 for S_A and S_B, respectively) as was the buffering capacity. The pH changes simulated with these groundwater compositions are

reported in the lower panels of Fig. 11. The metrics considered – total pH change and minimum pH – show very similar patterns in the two cases, indicating low sensitivity of groundwater pH to changes in sulphates. For S_A, the pH initially changed more rapidly because of the higher dechlorination rate due to the lack of competing TEAs. However, the pH change in the two scenarios reached almost the same maximum value and at the same time. The reason is that acidification is mainly controlled by the acetic acid production (fermentation reaction), which is not influenced by the sulphate concentration. As already presented, the model results show that for the set-up simulated that the fermentable substrate was consumed completely after about 100 d, and production of organic acids and electron donor stopped. The situation could vary when the fermentable substrate is available in excess and sulphates can be reduced completely. In this case, a larger dechlorination rate would be expected, with a higher rate of acidity production.

5. Summary and conclusions

A biogeochemical process-based model was developed to simulate the pH changes occurring during enhanced reductive dechlorination. One key advantage of the approach is that the model is flexible with respect to the chlorinated compounds undergoing remediation, and so its applicability is not restricted to chlorinated ethenes. In addition, while it does not attempt to simulate in full detail all the parent-daughter transformations, it retains enough complexity to account for pH-sensitive processes while remaining computationally inexpensive such that application to field sites is a realistic prospect.

A detailed model application was performed for the AAFB site. Abiotic reduction of chlorinated ethenes through iron sulphide oxidation was not considered because at the AAFB site there was no evidence that this process was taking place in parallel to bioremediation. At sites where abiotic degradation occurs, the model presented here should be extended to

include the amount of hydrochloric and sulphuric acids produced. At the AAFB site, the model was used to investigate pH changes and the geochemical signature of dechlorination along a single flow path. The model was calibrated successfully and was demonstrated to reproduce the observed long-term variations of pH and the parallel build-up of organic acids and reaction products. Modelling results indicate that, at the AAFB site, groundwater acidification near the injection wells resulted mainly from the accumulation of organic acids (by-products of the fermentation reaction), rather than hydrochloric acid produced by dechlorination. At a short distance from the injection barrier, the concentration of organic acids was small and the pH remained in the neutral range. Measurements of the individual chlorinated ethenes and the model showed that most of the parent chlorinated solvents were removed. Simulations showed, however, that near the injection wells the pH drop reduced biomass activity and dechlorination rates. At this site, the effect of groundwater acidification is mild and limited to the zone with higher concentration of fermentable substrate.

Since the fermentation reaction is independent of local geochemical conditions (e.g., presence of competing TEAs), it is expected that in many situations the accumulation of organic acids will be a major source of groundwater acidity. This suggests that the fermentable substrate injection scheme should be designed to minimize the build-up of organic acids.

A detailed analysis of the sensitivity of the microbial reactions to pH changes was not possible due to the limited available data from the AAFB site. The sensitivity analysis conducted demonstrated, however, the dramatic difference in terms of dechlorination when a more restrictive target pH is required. For this reason, the optimal pH for the dechlorination reaction in the field should be identified, in particular considering the pH sensitivity of the transformation of DCE to VC, and of VC to ethene.

A sensitivity analysis on the main processes controlling the extent of pH change was also conducted to study feedbacks on the dechlorination process and remediation efficiency. It was observed, not surprisingly, that a large pH change occurs when the characteristic rate for advective transport (denominator of Eqs. 18-19) is much less than the characteristic rate of the biological transformations (numerator of Eqs. 18-19). When the two time scales are similar or advective transport is dominant, the fermentation products are flushed out of the treatment zone, resulting in limited dechlorination (due to the lack of electron donor) and a limited pH change. This suggests that there is an optimal flow rate for which the dechlorination efficiency is maximized. In terms of engineering design, the hydraulic gradient is an adjustable factor. These results indicate that increasing the flow rate in the aquifer by pumping might alleviate the acidification problem, with the model used as a tool to define the optimal pumping rate and design a suitable remediation strategy. The pumping rate should provide a balance between dilution of fermentation/dechlorination products and sufficient residence time of the electron donor. Further investigation, however, is required to delineate fully the implications of this approach on the biogeochemical processes responsible for dechlorination (e.g., enhancing NAPL dissolution, decreasing residence time of chlorinated compounds in the treatment zone, etc.). Moreover, the effect of hydraulic conductivity heterogeneity remains to be examined.

For the field site examined, the small amount of calcite in the soil means that soil carbonates provided limited buffering. However, simulations confirmed that site clean-up is more effective when soluble carbonates are available, and that the pH change remains limited. Simulations with higher calcite content are equivalent to considering the circulation of an external buffer, and confirm that injection of an external source of buffer assists in sustaining microbial reactions, as previously reported [e.g., 6, 7, 51]. In this work, a 1D case with a homogeneous flow field was considered. In reality, a heterogeneous distribution of both the

hydraulic properties and the geochemical components (NAPL, soil minerals, etc.) complicates the treatment process. For example, one can expect that an injected buffer distribution would be dominated by preferential flow paths and be diffusion-limited in low permeability zones. Whether the injected buffer would be effective in limiting the extent of pH change would then depend on the spatial distribution of the NAPL, dechlorination rates, minerals, and the reaction rates of competing TEAPs. This results in a complex system, and its effects and consequences in terms of remediation efficiency need to be addressed in future studies. Notwithstanding this, the model presented here has been shown to capture the overall trends in the geochemical evolution of an engineered chlorinated solvent subsurface remediation scheme; thus, it could be applied to aid the design of such schemes.

6. Acknowledgements

We acknowledge support from BBSRC through the Bioremediation LINK Program (BB/B519076/1) and SNF 667 200021_120160.

References

[1] Cope N, JB Hughes. Biologically-enhanced removal of PCE from NAPL source zones. Environmental Science and Technology 2001;35:2014-21, doi:10.1021/es0017357.

[2] Yang Y, PL McCarty. Biologically enhanced dissolution of tetrachloroethene DNAPL. Environmental Science and Technology 2000;34:2979-89, doi:10.1021/es991410u.

[3] Leeson A, Becvar E, Henry B, Fortenberry J, Principles and Practices of Enhanced Anaerobic Bioremediation of Chlorinated Solvents. Technical report TR-2250-ENV. US Department of Defense, Air Force Center for Environmental Excellence and the Environmental Security Technology Certification Program (ESTCP). Arlington, VA, USA, 2004, pp. 457. http://www.dtic.mil/cgi-

bin/GetTRDoc?Location=U2&doc=GetTRDoc.pdf&AD=ADA511850, last accessed 6 April 2012.

[4] Adamson DA, DY Lyon, JB Hughes. Flux and product distribution during biological treatment of tetrachloroethene dense non-aqueous-phase liquid. Environmental Science and Technology 2004;38:2021-8, doi:10.1021/es034737a.

[5] Chu M, PK Kitanidis, PL McCarty. Possible factors controlling the effectiveness of bioenhanced dissolution of non-aqueous phase tetrachloroethene. Advances in Water Resources 2004;27:601-15, doi:10.1016/j.advwatres.2004.03.002.

[6] McCarty PL, MY Chu, PK Kitanidis. Electron donor and pH relationships for biologically enhanced dissolution of chlorinated solvent DNAPL in groundwater. European Journal of Soil Science 2007;43:276-82, doi:10.1016/j.ejsobi.2007.03.004.

[7] Robinson C, DA Barry, PL McCarty, JI Gerhard, I Kouznetsova. pH control for enhanced reductive bioremediation of chlorinated solvent source zones. Science of the Total Environment 2009;407:4560-73, doi:10.1016/j.scitotenv.2009.03.029.

[8] Da Silva MLB, RC Daprato, DE Gomez, JB Hughes, CH Ward, PJJ Alvarez. Comparison of bioaugmentation and biostimulation for the enhancement of dense nonaqueous phase liquid source zone bioremediation. Water Environment Research 2006;78:2456-65, doi:10.2175/106143006X123111.

[9] Middeldorp PJM, MLGC Luijten, BA van de Pas, MHA van Eekert, SWM Kengen, G Schraa, et al. Anaerobic microbial reductive dehalogenation of chlorinated ethenes. Bioremediation Journal 1999;3:151-69, doi:10.1080/10889869991219280.

[10] Sleep BE, DJ Seepersad, K Mo, CM Heidorn, L Hrapovic, PL Morrill, et al. Biological enhancement of tetrachloroethene dissolution and associated microbial community changes. Environmental Science and Technology 2006;40:3623-33, doi:10.1021/es051493g.

[11] Cirpka OA, C Windfuhr, G Bisch, S Granzow, H Scholz-Muramatsu, H Kobus. Microbial reductive dechlorination in large-scale sandbox model. Journal of Environmental Engineering 1999;125:861-70.

[12] Lacroix E, A Brovelli, C Holliger, DA Barry. Evaluation of silicate minerals for pH control during bioremediation: Application to chlorinated solvents. In press, Water, Air, & Soil Pollution doi:10.1007/s11270-011-1058-4.

[13] Damborsky J. Tetrachloroethene-dehalogenating bacteria. Folia Microbiologica 1999;44:247-62, doi:10.1007/BF02818543.

[14] Holliger C, G Schraa, AJM Stams, AJB Zehnder. A highly purified enrichment culture couples the reductive dechlorination of tetrachloroethene to growth. Applied and Environmental Microbiology 1993;59:2991-7.

[15] Neumann A, H Scholz-Muramatsu, G Diekert. Tetrachloroethene metabolism of Dehalospirillum multivorans. Archives of Microbiology 1994;162:295-301, doi:10.1007/BF00301854.

[16] Robinson C, DA Barry. Design tool for estimation of buffer requirement for enhanced reductive dechlorination of chlorinated solvents in groundwater. Environmental Modelling & Software 2009;24:1332-8, doi:10.1016/j.envsoft.2009.03.012.

[17] Kouznetsova I, X Mao, C Robinson, DA Barry, JI Gerhard, PL McCarty. Biological reduction of chlorinated solvents: Batch-scale geochemical modeling. Advances in Water Resources 2010;33:969-86, doi:10.1016/j.advwatres.2010.04.017.

[18] Clement TP, CD Johnson, Y Sun, GM Klecka, C Bartlett. Natural attenuation of chlorinated ethene compounds: Model development and field-scale application at the Dover site. Journal of Contaminant Hydrology 2000;42:113-40, doi:10.1016/S0169-7722(99)00098-4.

[19] Lee IS, JH Bae, PL McCarty. Comparison between acetate and hydrogen as electron donors and implications for the reductive dehalogenation of PCE and TCE. Journal of Contaminant Hydrology 2007;94:76-85, doi:10.1016/j.jconhyd.2007.05.003.

[20] Dolfing J, JM Tiedje. Acetate as a source of reducing equivalents in the reductive dechlorination of 2,5-dichlorobenzoate. Archives of Microbiology 1991;156:356-61, doi:10.1007/BF00248710.

[21] Sung Y, KE Fletcher, KM Ritalahti, RP Apkarian, N Ramos-Hernández, RA Sanford, et al. Geobacter lovleyi sp. nov. strain SZ, a novel metal-reducing and tetrachloroethene-dechlorinating bacterium. Applied and Environmental Microbiology 2006;72:2775-82, doi:10.1128/AEM.72.4.2775-2782.2006.

[22] Zhuang P, SG Pavlostathis. Effect of temperature, pH and electron donor on the microbial reductive dechlorination of chloroalkenes. Chemosphere 1995;31:3537-48, doi:10.1016/0045-6535(95)00204-L.

[23] Kennedy LG, JW Everett, J Gonzales. Assessment of biogeochemical natural attenuation and treatment of chlorinated solvents, Altus Air Force Base, Altus, Oklahoma. Journal of Contaminant Hydrology 2006;83:221-36, doi:10.1016/j.jconhyd.2005.11.006.

[24] He YT, JT Wilson, RT Wilkin. Impact of iron sulfide transformation on trichloroethylene degradation. Geochimica et Cosmochimica Acta 2010;74:2025-39, doi:10.1016/j.gca.2010.01.013.

[25] Butler EC, KF Hayes. Factors influencing rates and products in the transformation of trichloroethylene by iron sulfide and iron metal. Environmental Science and Technology 2001;35:3884-91, doi:10.1021/es010620f.

[26] Clement TP, TR Gautam, KK Lee, MJ Truex, GB Davis. Modeling of DNAPL-dissolution, rate-limited sorption and biodegradation reactions in groundwater systems. Bioremediation Journal 2004;8:47-64, doi:10.1080/10889860490453177.

[27] Wiedemeier TH, HS Rifai, JT Wilson, C Newell. Natural attenuation of fuels and chlorinated solvents in the subsurface. John Wiley, New York, 1999.

[28] Brun A, P Engesgaard. Modelling of transport and biogeochemical processes in pollution plumes: Literature review and model development. Journal of Hydrology 2002;256:211-27, doi:10.1016/S0022-1694(01)00547-9.

[29] Jakobsen R, D Postma. Redox zoning, rates of sulphate reduction and interactions with Fe-reduction and methanogenesis in a shallow sandy aquifer, Romo, Denmark. Geochimica et Cosmochimica Acta 1999;63:137-51, doi:10.1016/S0016-7037(98)00272-5.

[30] Parkhurst DL, CAJ Appelo. User's Guide to PHREEQC (Version 2) – A Computer Program for Speciation, Batch-Reaction, One-Dimensional Transport, and Inverse Geochemical Calculations, Water-Resources Investigations Report 99-4259. US Geological Survey, Denver, Colorado, USA, 1999. http://wwwbrr.cr.usgs.gov/projects/GWC_coupled/phreeqc/, last accessed 5 April 2012.

[31] Maurer M, BE Rittmann. Formulation of the CBC-model for modelling the contaminants and footprints in natural attenuation of BTEX. Biodegradation 2004;15:419-34, doi:10.1023/B:BIOD.0000044589.40735.b0.

[32] Ratkowsky DA, T Ross. Modelling the bacterial growth/no growth interface. Letters in Applied Microbiology 1995;20:29-33, doi:10.1111/j.1472-765X.1995.tb00400.x.

[33] Paul EA, FE Clark. Soil microbiology and biochemistry. 2nd ed. Academic Press, San Diego, California, USA, 1996.

[34] Brusseau ML, Z Zhang, NT Nelson, RB Cain, GR Tick, M Oostrom. Dissolution of nonuniformly distributed immiscible liquid: Intermediate-scale experiments and mathematical modeling. Environmental Science and Technology 2002;36:1033-41, doi:10.1021/es010609f.

[35] Dekker TJ, LM Abriola. The influence of field-scale heterogeneity on the surfactant-enhanced remediation of entrapped nonaqueous phase liquids. Journal of Contaminant Hydrology 2000;42:219-51, doi:10.1016/S0169-7722(99)00091-1.

[36] Zhang Z, ML Brusseau. Nonideal transport of reactive solutes in heterogeneous porous media 5. Simulating regional-scale behavior of a trichloroethene plume during pump-and-treat remediation. Water Resources Research 1999;35:2921-35, doi:10.1029/1999WR900162.

[37] Powers SE, LM Abriola, JS Dunkin, WJ Weber Jr. Phenomenological models for transient NAPL-water mass-transfer processes. Journal of Contaminant Hydrology 1994;16:1-33, doi:10.1016/0169-7722(94)90070-1.

[38] Powers SE, CO Loureiro, LM Abriola, WJ Weber Jr. Theoretical study of the significance of nonequilibrium dissolution of nonaqueous phase liquids in subsurface systems. Water Resources Research 1991;27:463-77, doi:10.1029/91WR00074.

[39] Appelo CAJ, D Postma. Geochemistry, Groundwater and Pollution. 2nd ed. A. A. Balkema Publishers, Amsterdam, Netherlands, 2005.

[40] Bräuer SL, JB Yavitt, SH Zinder. Methanogenesis in McLean Bog, an acidic peat bog in upstate New York: Stimulation by H_2/CO_2 in the presence of Rifampicin, or by low concentrations of acetate. Geomicrobiology Journal 2004;21:433-43, doi:10.1080/01490450490505400.

[41] van Kessel JAS, JB Russell. The effect of pH on ruminal methanogenesis. FEMS Microbiology Ecology 1996;20:205-10, doi:10.1111/j.1574-6941.1996.tb00319.x.

[42] Russell JB. Intracellular pH of acid-tolerant ruminal bacteria. Applied and Environmental Microbiology 1991;57:3383-4.

[43] Staley BF, FL de los Reyes, III, MA Barlaz. Effect of spatial differences in microbial activity, pH, and substrate levels on methanogenesis initiation in refuse. Applied and Environmental Microbiology 2011;77:2381-91, doi:10.1128/AEM.02349-10.

[44] Yang Y, PL McCarty. Comparison between donor substrates for biologically enhanced tetrachloroethene DNAPL dissolution. Environmental Science & Technology 2002;36:3400-4, doi:10.1021/es011408e.

[45] Plummer LN, TML Wigley, DL Parkhurst. The kinetics of calcite dissolution in CO_2 -water systems at 5 degrees to 60 degrees C and 0.0 to 1.0 atm CO_2. American Journal of Science 1978;278:179-216.

[46] Roden EE, MM Urrutia. Influence of biogenic Fe(II) on bacterial crystalline Fe(III) oxide reduction. Geomicrobiology Journal 2002;19:209-51, doi:10.1080/01490450252864280.

[47] Roden EE, MM Urrutia, CJ Mann. Bacterial reductive dissolution of crystalline Fe(III) oxide in continuous-flow column reactors. Applied and Environmental Microbiology 2000;66:1062-5, doi:10.1128/AEM.66.3.1062-1065.2000.

[48] Tournassat C, P Alt-Epping, EC Gaucher, T Gimmi, OX Leupin, P Wersin. Biogeochemical processes in a clay formation in situ experiment: Part F - Reactive transport modelling. Applied Geochemistry 2011;26:1009-22, doi:10.1016/j.apgeochem.2011.03.009.

[49] Stumm W, JJ Morgan. Aquatic Chemistry: Chemical Equilibria and Rates in Natural Waters. Third ed. John Wiley & Sons, New York, USA, 1996.

[50] Dzombak DA, FMM Morel. Surface Complexation Modeling: Hydrous Ferric Oxide. Wiley and Sons, New York, USA, 1990.

[51] Borden RC, MT Lieberman, MD Lee. Technology Application of Low Cost Emplacement of Insoluble Organic Substrate for Enhanced in situ Reductive Cechlorination of Halogenated Aliphatic Hydrocarbons: Altus Air Force Base, Altus, Oklahoma. Air Force Center for Environmental Excellence, San Antonio, Texas, USA, 2004. pp. 41.

http://www.afcee.af.mil/shared/media/document/AFD-071203-119.pdf, last accessed 5 April 2012.

[52] Lee MD, MT Lieberman, W Beckwith, RC Borden, J Everett, L Kennedy, et al. Pilots to enhance trichloroethene reductive dechlorination and ferrous sulfide abiotic transformation. in: VS Magar, ME Kelley, (Eds.). Proceedings of the Seventh International in Situ and On-Site Bioremediation Symposium. Battelle Press, Orlando, Florida, USA, 2003.

[53] Parsons I. Final Workplan for in-situ Bioremediation of Chlorinated Aliphatic Hydrocarbons using a Permeable Reactive Biowall. Operable Unit 1. Altus Air Force Base, Oklahoma. Air Force Center for Environmental Excellence, San Antonio, Texas, USA, 2002. pp. 171. http://www.afcee.af.mil/shared/media/document/AFD-071203-109.pdf, last accessed 5 April 2012.

[54] Parkhurst DL, KL Kipp, P Engesgaard, SR Charlton. PHAST-A Program for Simulating Ground-water Flow, Solute Transport, and Multicomponent Geochemical Reactions. US Geological Survey Techniques and Methods 6, Denver, Colorado, USA, 2004. pp. 154. http://pubs.usgs.gov/tm/2005/tm6A8/#pdf, last accessed 5 April 2012.

[55] Christ JA, LM Abriola. Modeling metabolic reductive dechlorination in dense non-aqueous phase liquid source-zones. Advances in Water Resources 2007;30:1547-61, doi:10.1016/j.advwatres.2006.05.024.

[56] Lee IS, JH Bae, Y Yang, PL McCarty. Simulated and experimental evaluation of factors affecting the rate and extent of reductive dehalogenation of chloroethenes with glucose. Journal of Contaminant Hydrology 2004;74:313-31, doi:10.1016/j.jconhyd.2004.03.006.

[57] Clapp LW, MJ Semmens, PJ Novak, RM Hozalski. Model for in situ perchloroethene dechlorination via membrane-delivered hydrogen. Journal of Environmental Engineering 2004;130:1367-81.

Tables

Table 1

Parameters and correlation coefficients of the fitted logistic functions used to model pH inhibition.

Parameter	I_{pH}^{HN}	I_{pH}^{Z}	I_{pH}^{AFB}
M	11.97	14.26	6.2
D	6.72	6.98	6
v	0.8	0.05	0.28
Correlation coefficient, r^2	0.76	0.99	-

Table 2

Properties of the 1D transect model for the Altus Air Force Base remediation scheme.

Parameter	Value	Units	Source
Model length	15	m	[51, 52]
Average depth BGW[a]	2	m	[51, 52]
Temperature	20	°C	[51, 52]
Number of cells	60	-	-
Grid spacing	0.25	m	-
Average hydraulic gradient	3.5×10^{-3}	-	[51, 52][b]
Hydraulic conductivity	10^{-1}	m d^{-1}	[51, 52][b]
Effective porosity	0.35	-	[51, 52][b]
Longitudinal dispersivity	0.2	m	Assumed

[a]Average depth below groundwater level: Defines the threshold pressure for gas bubbling

[b]Average value for the area considered in the model

Table 3

Average groundwater composition at Pilot Test #1, AAFB.

Constituent	Value	Units	Source
pH	7.1	-	[51]
Alkalinity (as $CaCO_3$)	320	mg l^{-1}	[53]
SO_4^{2-}	1536	mg l^{-1}	[51]
S^{2-}	0	mg l^{-1}	[51]
Soluble iron	0	mg l^{-1}	[51]
Dissolved oxygen	0.5	mg l^{-1}	[51]
Total organic carbon	5.63	mg l^{-1}	[51]
Br^-	2.97	mg l^{-1}	[51]
Cl^-	600	mg l^{-1}	[51]
Ca^{2+}	350	mg l^{-1}	Assumed*
K^+	200	mg l^{-1}	Assumed*
Na^+	300	mg l^{-1}	Assumed*
Mg^{2+}	240	mg l^{-1}	Assumed*
Mn^{2+}	0.27	mg l^{-1}	[53]

*Major cations not measured. Values computed in order to achieve electrical balance of the solution. Modelling results are not sensitive to these components.

Table 4

Initial concentration of the immobile components.

Component	Value	Units	Source
$CaCO_3$ (s)	10^{-3}	mol (kg water)$^{-1}$	Assumed
R-Cl (s)	-	mol (kg water)$^{-1}$	Assumed
B_F	10^{-3}	g (kg water)$^{-1}$	Assumed
B_D	10^{-4}	g (kg water)$^{-1}$	[55, 56]
Bioavailable[a] total iron	3.55	g (kg soil)$^{-1}$	[51, 52]
Ferrihydrite[*]	30%	-	Calibrated
Goethite[*]	70%	-	Calibrated
Hfo, weak sites	0.2	mol (mol Fe) $^{-1}$	[50]
Hfo, strong sites	0.005	mol (mol Fe) $^{-1}$	[50]
Hfo, surface area[c]	222	m^2 g^{-1}	[39]

[a] Extracted with weak acid (0.5 N HCl)

[*] Fraction of the bio-available iron oxides in the soil

[c] Average value considering the relative proportions of ferrihydrite and goethite

Table 5

Parameters for the biogeochemical model, and corresponding ranges taken from the literature. Note that the parameters taken from the literature are average values for TCE and DCE.

Parameter	Value	Units	Source	Range	Sources
κa_0	5×10^{-3}	d^{-1}	Calibrated		
β_F	1	-	[21]		
$C_{aq,F}^{eq}$	5×10^{-2}	mol l^{-1}	Calibrated		
$\mu_{max,F}$	5×10^{-2}	mol (g biomass)$^{-1}$ d^{-1}	Calibrated	$10^{-3} - 5 \times 10^{-2}$	[17, 31, 55, 57]
$K_{h,F}$	10^{-5}	mol l^{-1}	Assumed	1.7×10^{-5}	[17, 31]
$\mu_{max,D}$	10^{-4}	mol (g biomass)$^{-1}$ d^{-1}	Calibrated	$10^{-4} - 5 \times 10^{-3}$	[17, 55, 57]
$K_{h,D}$	5×10^{-4}	mol l^{-1}	Assumed	$2 \times 10^{-7} - 10^{-3}$	[17, 55, 57]
K_{h,H_2}	2×10^{-9}	mol l^{-1}	[17]		
$K_{h,Acetate}$	10^{-5}	mol l^{-1}	Assumed		
k_d	5×10^{-2}	d^{-1}	[19]		
Y_F	5	(g cell)(mol R-Cl)$^{-1}$	Calibrated	1.6 – 6	[17, 55, 57]

Y_D	2.5	(g cell)(mol R-Cl)$^{-1}$	Calibrated	2.3 – 11.7	[17, 55, 57]
$r_{d,min}$	0.1	-	Calibrated	0.1 – 0.5	[3]
$\mu_{max,A}$	1.25×10^{-4}	mol (g biomass)$^{-1}$ d^{-1}	Calibrated	$110^{-4} - 8 \times 10^{-2}$	[17, 31]
$\mu_{CH_4,\ CH_3COOH}$	8×10^{-7}	d^{-1}	Calibrated		
$\mu_{CH_4,\ H_2}$	6×10^{-7}	d^{-1}	Calibrated		
C_{RCl}^{switch}	3×10^{-3}	mol l^{-1}	[2]		

Figures

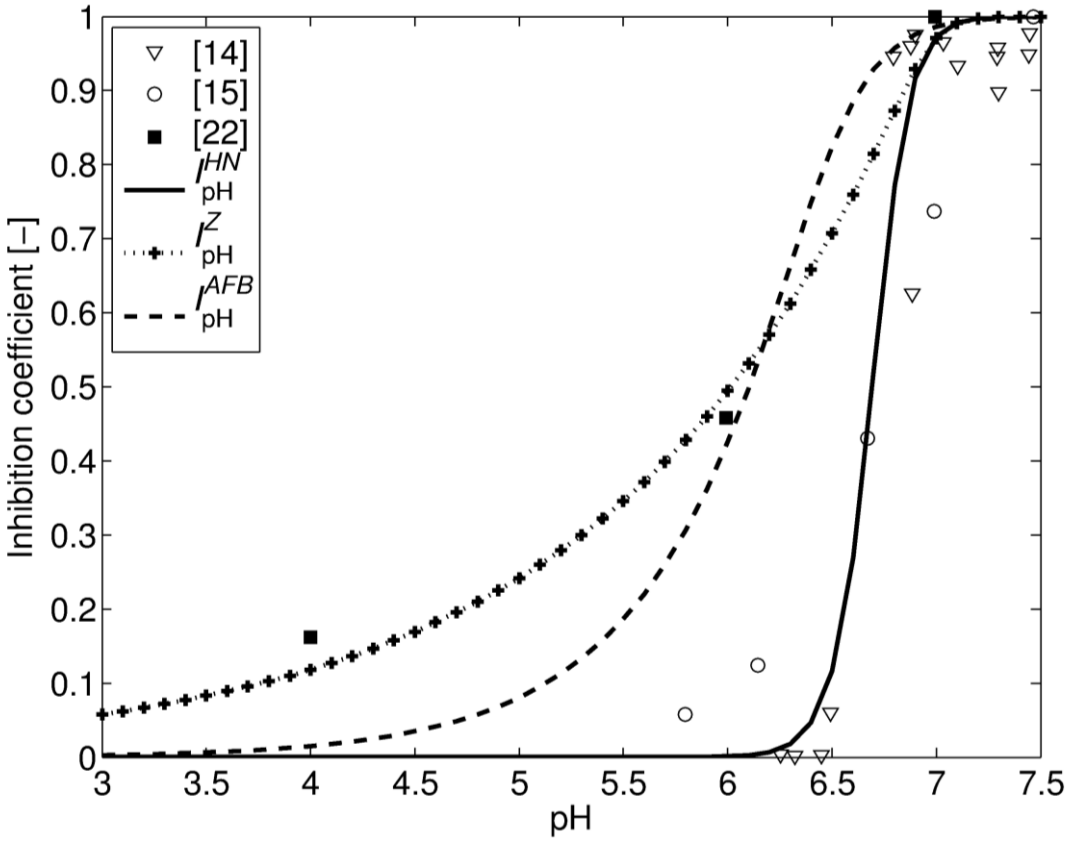

Fig. 1. Experimental data (symbols) and fitted pH inhibition functions. The inhibition functions I_{pH}^{HN} and I_{pH}^{Z} are optimised least-squares fits of the data. I_{pH}^{AFB} (dashed line) was fitted by trial-and-error to reproduce the field measurements at the Altus Air Force Base.

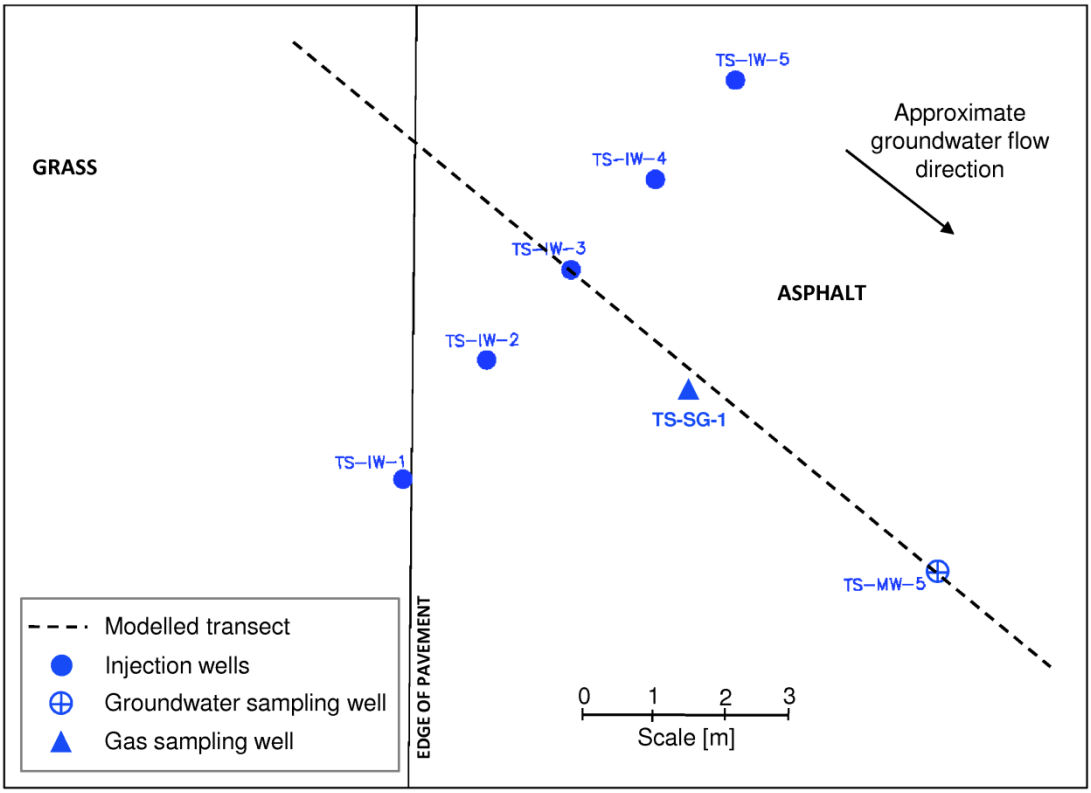

Fig. 2. Layout of the AAFB Plot 1 (after [33]). The dashed line represents the location of the transect modelled in this work. Only the groundwater sampling well (TS-MW-5) relevant to this study is shown in addition to all the injection wells.

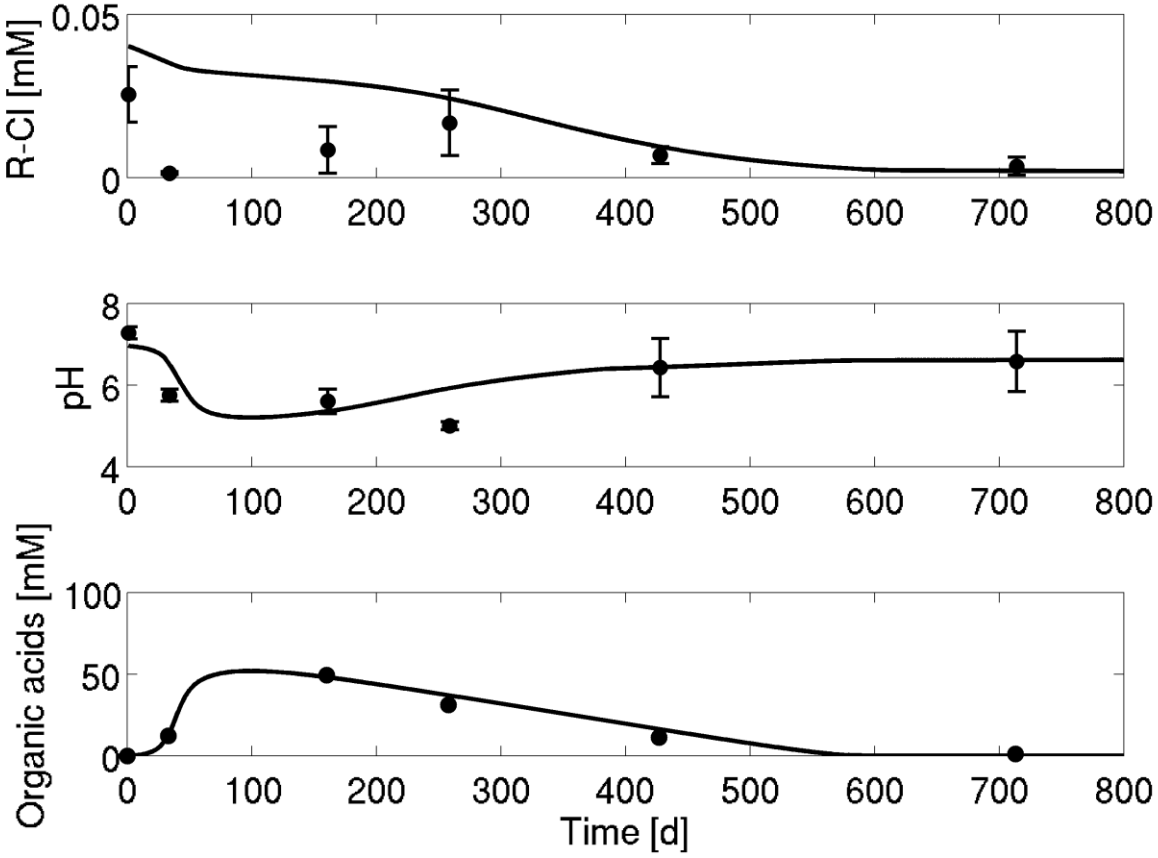

Fig. 3. Measured values (dots [33]) and model results of chlorinated ethenes, pH and fermentation products (organic acids) at the injection well. For R-Cl and pH, the average (± 1 s.d.) of all injection wells was used, while organic acids were measured at just one location. Chlorinated ethenes are shown as moles of R-Cl groups. The simulated pH evolution closely reproduces the field data, indicating that the modelling approach is suitable to study the build-up of acidity resulting from reductive dechlorination.

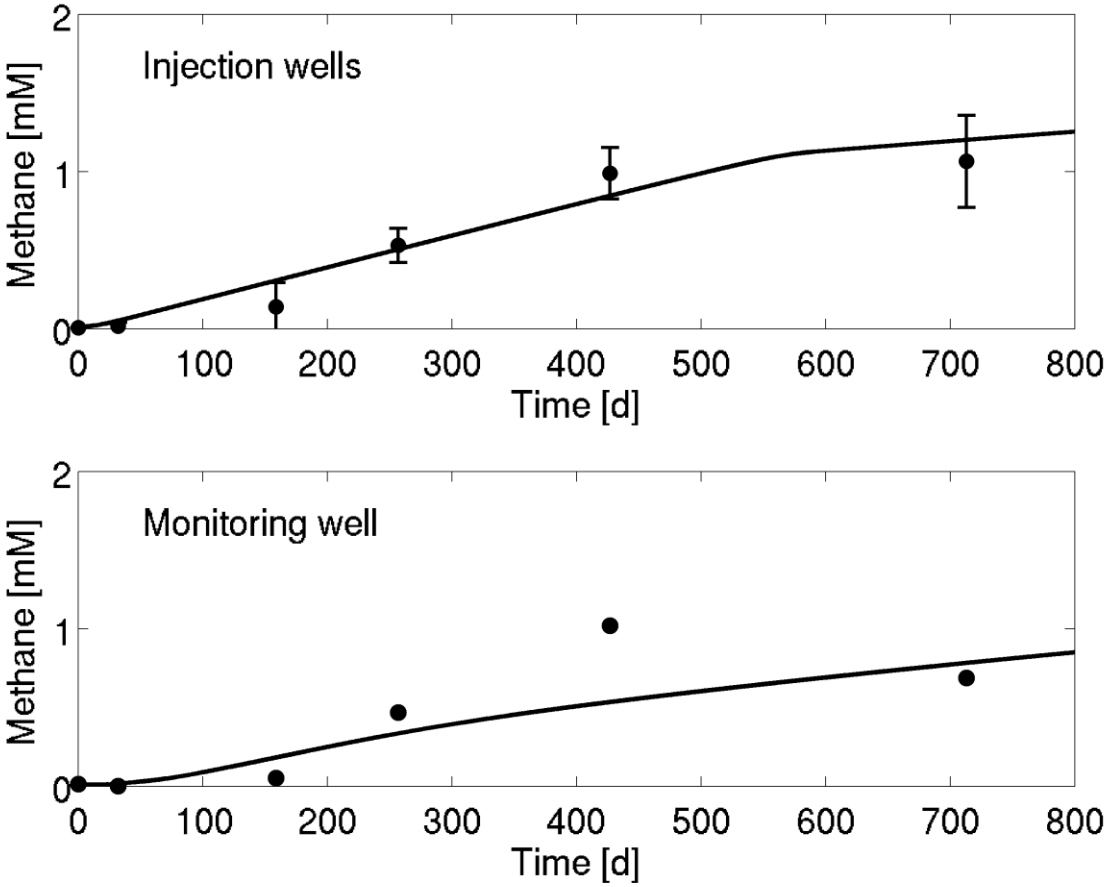

Fig. 4. Methane production at the injection and monitoring wells in the fields (closed circles) and simulations (solid line). The mean value and standard deviation of the measurements at all injection wells is reported. The model well reproduces the trends observed in the field.

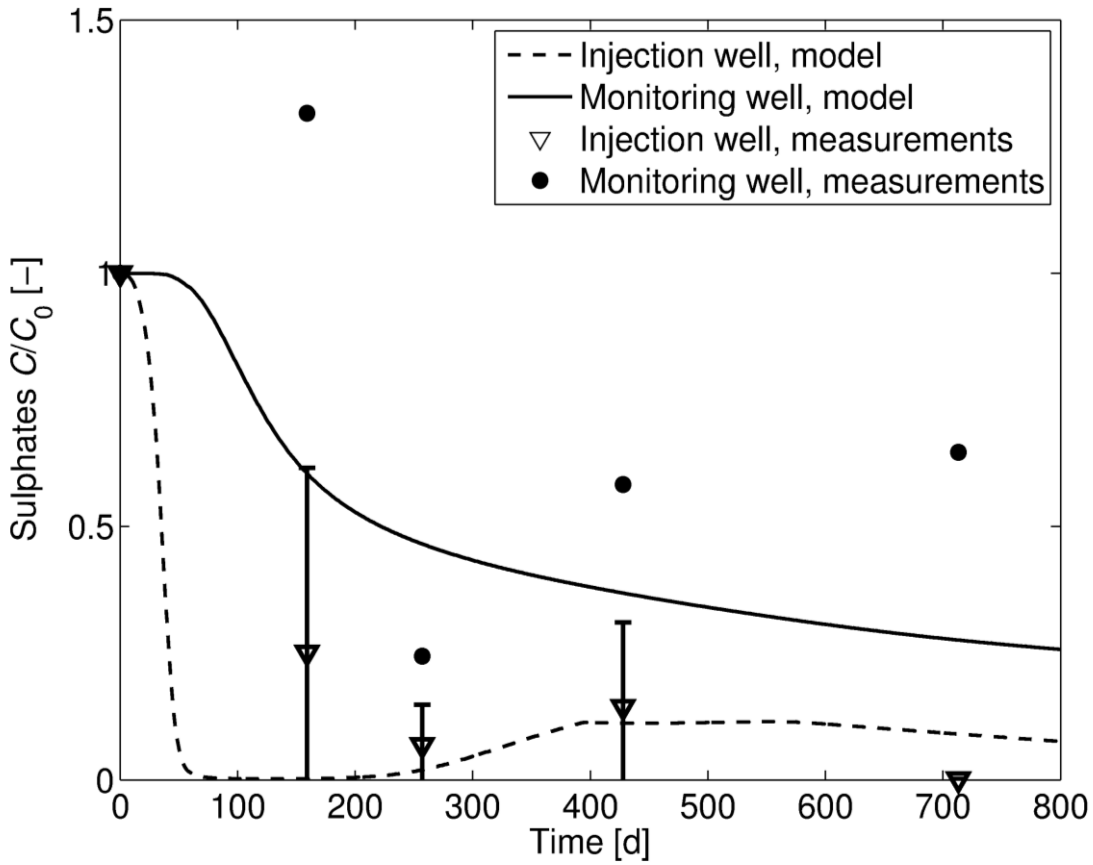

Fig. 5. Normalized concentration of sulphates as computed in the model (lines) and measured in the groundwater. The closed circles and the solid line are relevant to the monitoring well, while the open symbols (squares and triangles) and the broken line are for the injection well. The average concentrations and standard deviation of all the injection locations are reported (open triangle with the error bar). Simulation results reproduce the overall trend of sulphates near the injection barrier, while the comparison is less satisfactory at the monitoring well. This could be due to the highly heterogeneous distribution of sulphates in the area.

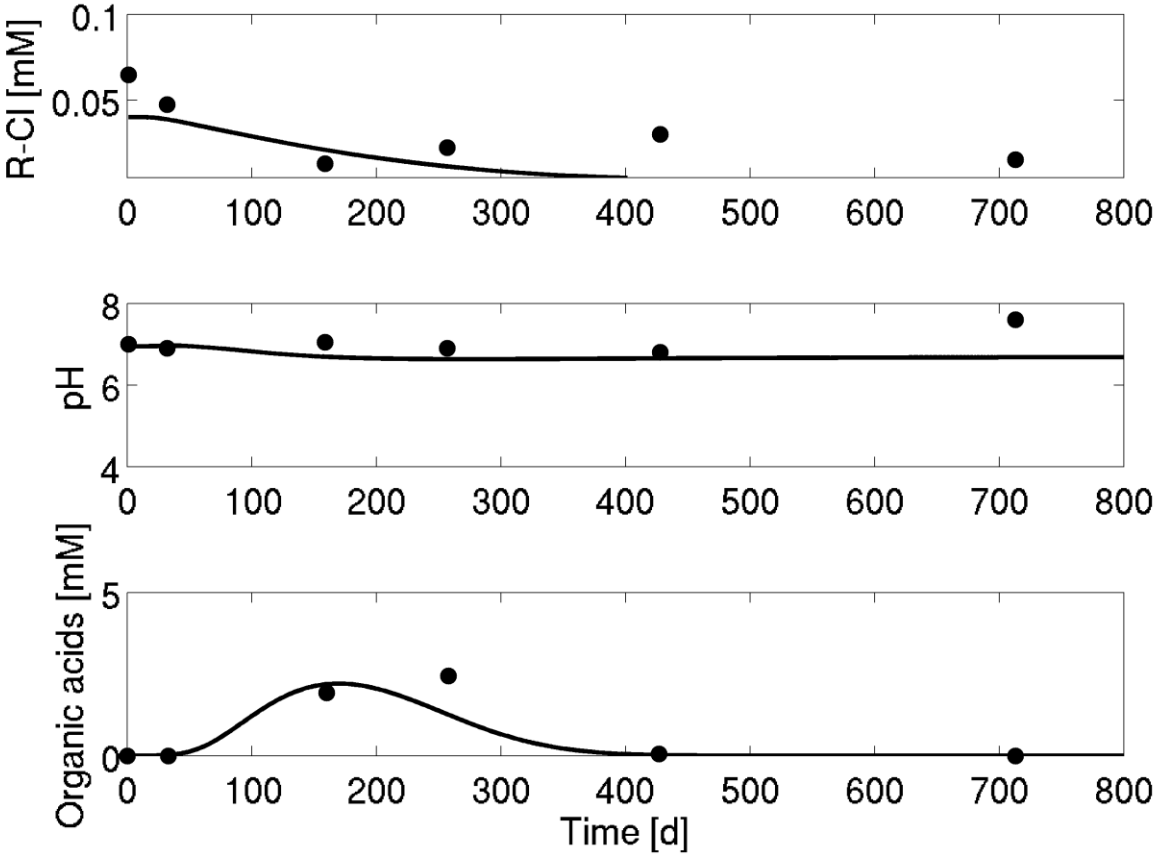

Fig. 6. Comparison of the modelled and measured concentrations of chlorinated ethenes, organic acids and pH at the downgradient monitoring well. The model reproduces the overall behaviour observed in the field well.

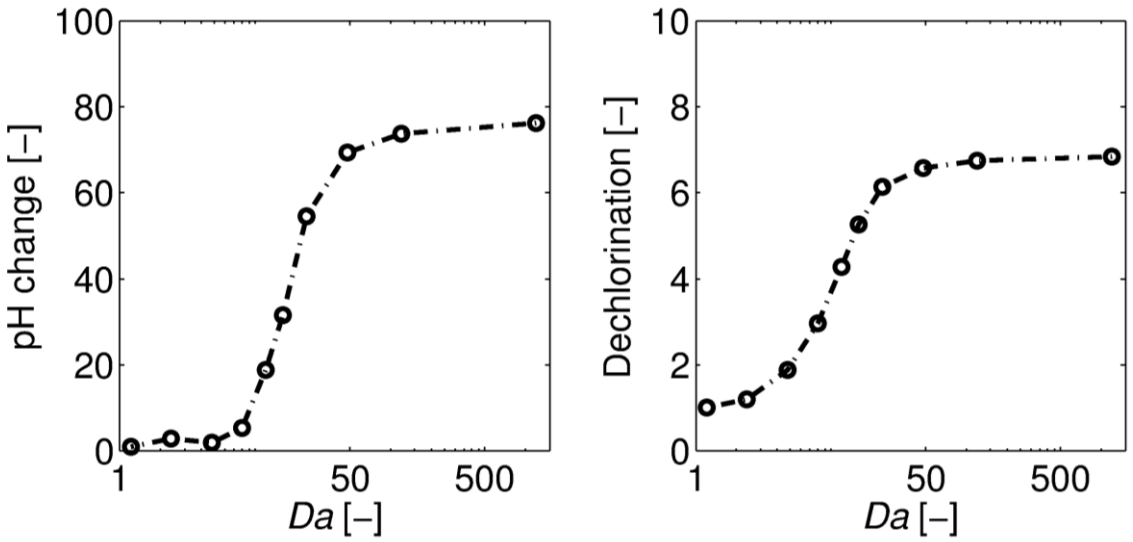

Fig. 7. Effect of the groundwater flow rate on the total dechlorination (Eq. 15) and extent of pH change (Eq. 16). The two metrics were normalized using their value at $Da = 1$. Note that *Da* is plotted on a logarithmic axis. As the Damköhler number increases (i.e., the reaction rate increases relative to the flow rate), both the extent of dechlorination and the pH change first increase (until $Da \approx 100$) then remain constant. At low *Da* the groundwater flow quickly removes the electron donor (H_2) produced from fermentation and dechlorination is limited by its availability. On the contrary, when the groundwater residence time is larger than the characteristic reaction time (high *Da*), reaction products accumulate and the pH drops. In this situation, dechlorination is inhibited by groundwater acidification.

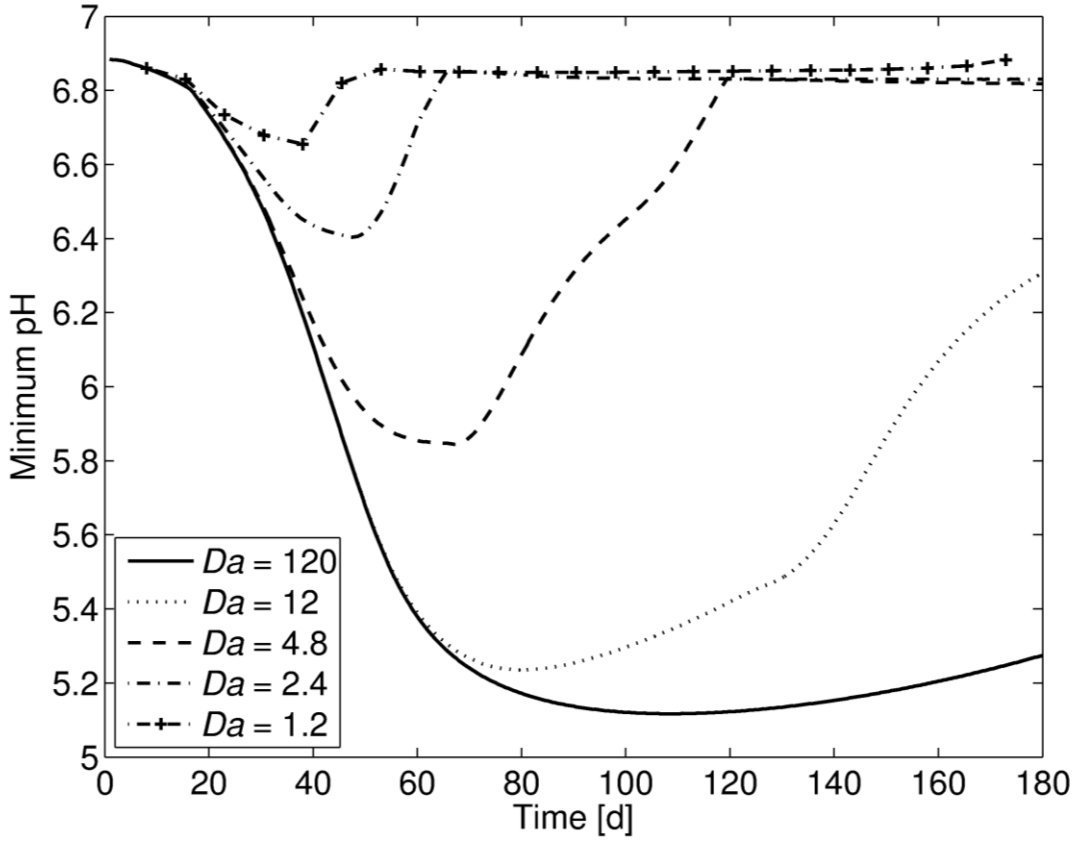

Fig. 8. Effect of the flow rate and Damköhler number on the groundwater pH: As the flow rate increases (*Da* decreases), the pH in the aquifer becomes less acidic. This is due to two synergetic mechanisms, (i) reduction of the dechlorination rate due to the removal of electron donor and (ii) wash-out of acids from the contaminated site.

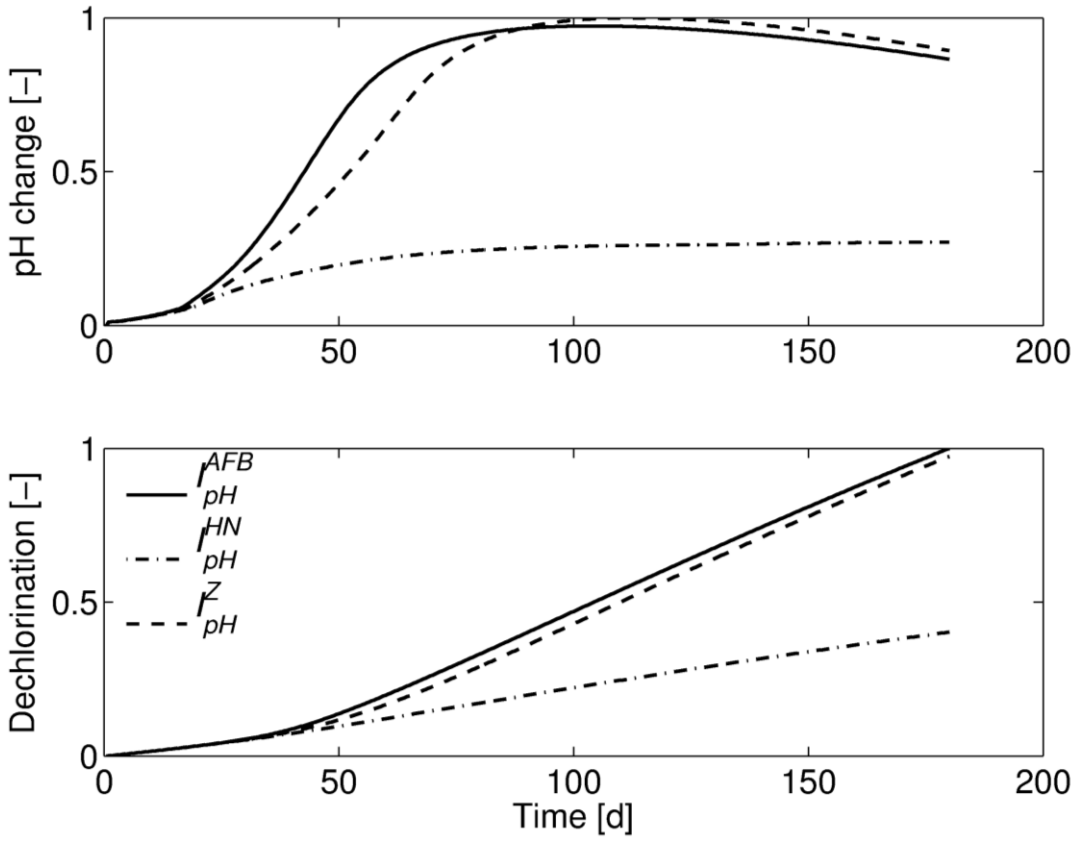

Fig. 9. Effect of the pH inhibition function on the extent of pH change (upper panel) and total dechlorination (lower panel). The metrics were normalized using the maximum value to facilitate the comparison. The solid line is the function assumed for the AAFB case, while the dashed line is the function fitted to the data from [22] and the dash-dot line is fitted to the data from [14] and [15]. The two behaviours observed in the laboratory experimental data result in significantly different behaviour in the field.

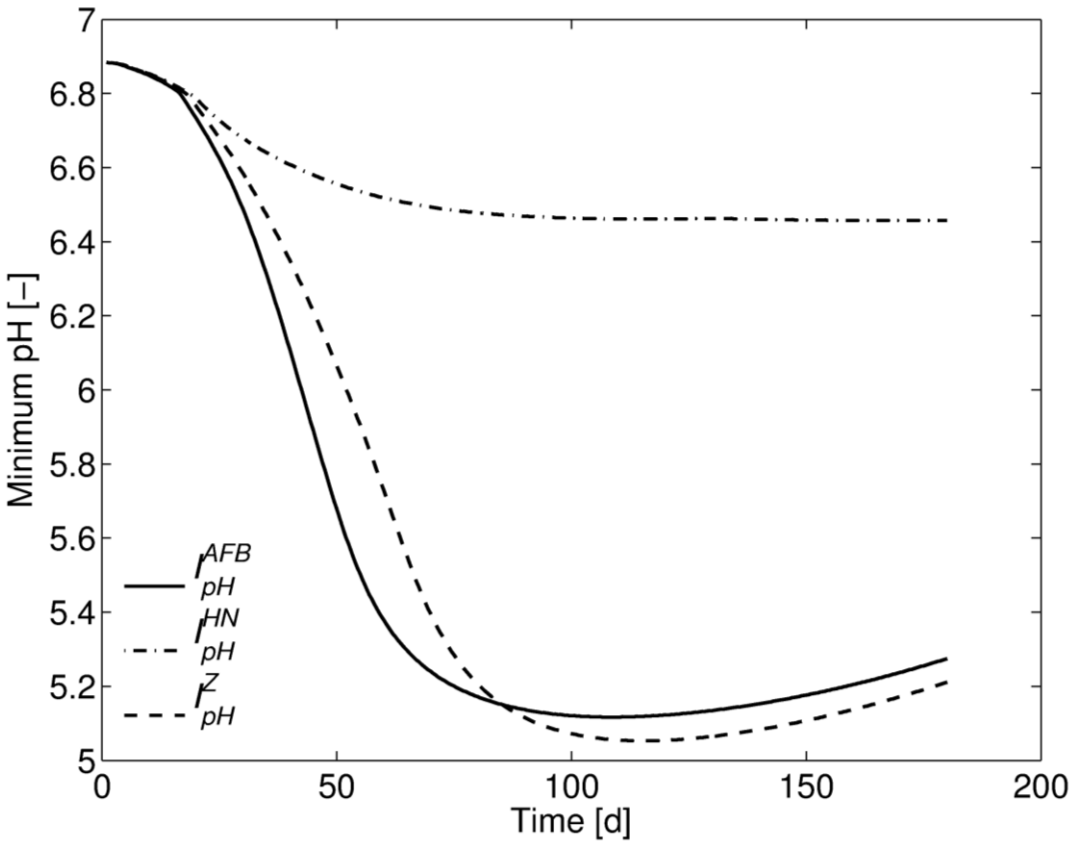

Fig. 10. Minimum pH in the simulations using different pH inhibition functions. The function calibrated to the AAFB data (I_{pH}^{AFB}) leads to a minimum pH close to that observed using the function from (I_{pH}^{Z}). This is because in this case the pH remains mainly above 5.5, where the two functions are very similar (Fig. 1). At lower pH values, the function obtained using the data from [31] predicts less inhibition and increased dechlorination relative the function adopted for the AAFB case.

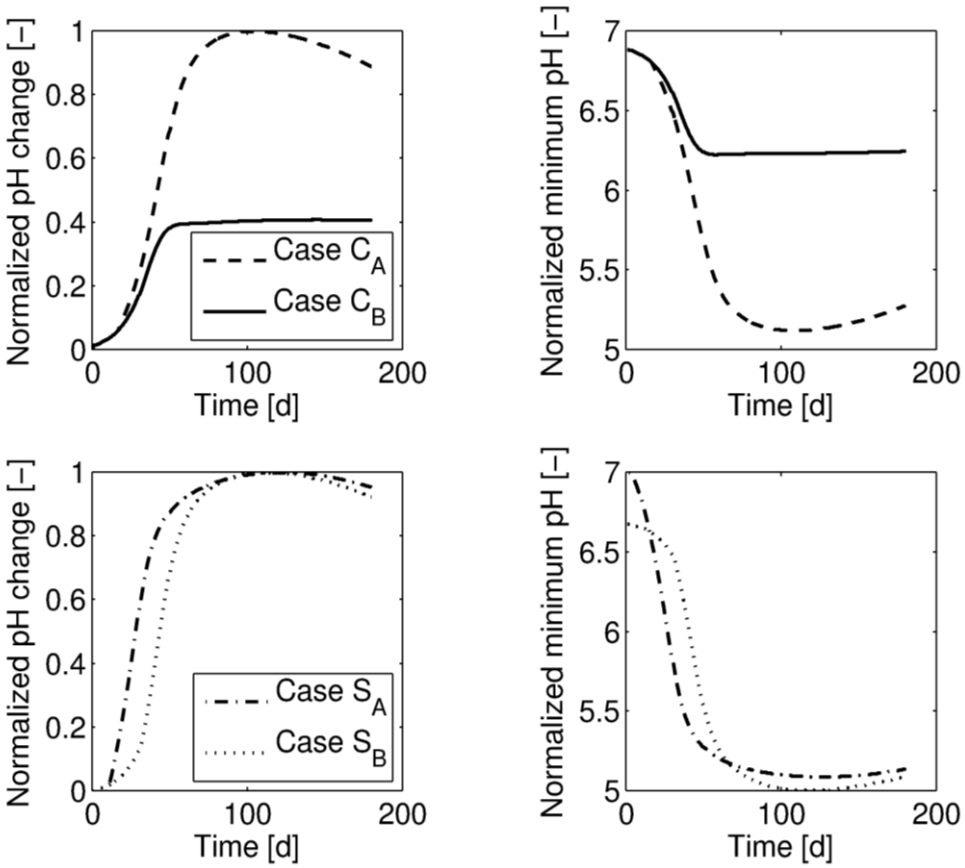

Fig. 11. Sensitivity of pH changes to soil calcite content (upper panels, Cases C_A and C_B) and dissolved sulphate concentration in groundwater (lower panels, Cases S_A and S_B, low and high sulphate concentration). The values of pH change were normalized using the maximum value. The buffering effect of calcite is shown by the comparison of cases C_A (low carbonates content) and C_B (high calcite content). In contrast, pH changes are only weakly sensitive to groundwater sulphate content, at least for the conditions considered here.